ORNL-4149
UC-80 – Reactor Technology

ANALYSIS OF NEUTRON FLUCTUATION SPECTRA IN THE OAK RIDGE RESEARCH REACTOR AND THE HIGH FLUX ISOTOPE REACTOR

J. C. Robinson

OAK RIDGE NATIONAL LABORATORY
operated by
UNION CARBIDE CORPORATION
for the
U.S. ATOMIC ENERGY COMMISSION

Printed in the United States of America. Available from Clearinghouse for Federal
Scientific and Technical Information, National Bureau of Standards,
U.S. Department of Commerce, Springfield, Virginia 22151
Price: Printed Copy $3.00; Microfiche $0.65

ORNL-4149

Contract No. W-7405-eng-26

INSTRUMENTATION AND CONTROLS DIVISION

ANALYSIS OF NEUTRON FLUCTUATION SPECTRA IN THE OAK RIDGE RESEARCH REACTOR AND THE HIGH FLUX ISOTOPE REACTOR

J. C. Robinson

OCTOBER 1967

OAK RIDGE NATIONAL LABORATORY
Oak Ridge, Tennessee
operated by
UNION CARBIDE CORPORATION
for the
U. S. ATOMIC ENERGY COMMISSION

CONTENTS

ANALYSIS OF NEUTRON FLUCTUATION SPECTRA IN THE OAK RIDGE RESEARCH REACTOR AND THE HIGH FLUX ISOTOPE REACTOR

J. C. Robinson*

ABSTRACT

An analytical model which accounted for distributed effects on reactivity due to the coolant and heat transport time was developed to aid in the study of the power spectral density of fluctuating current from a neutron-sensitive ionization chamber in the Oak Ridge Research Reactor (ORR) and the High Flux Isotope Reactor (HFIR). Results from the model led to the conclusion that feedback effects on the power spectral density (for these reactors) are small over the frequency range of observation. A comparison of the observed spectra (when properly normalized) at various power levels verified the analytical predictions; therefore, we concluded that the observed spectra were induced by a reactivity driving function(s) which was independent of the power level.

From a comparison of the observed spectra from the HFIR during the life of a given core, we concluded that the principal driving function was fluctuation of the control rods, which was assumed to be induced by coolant flow fluctuations. Furthermore, we observed that the control rods exhibited resonances at certain positions.

Spectra from the ORR at various rod positions were compared. We concluded that rod vibrations and fuel element vibrations were the driving functions. From spectra obtained at various coolant flow rates, it was clear that these vibrations were induced by fluctuations in the coolant velocity.

ACKNOWLEDGMENTS

The topic of this investigation was originally suggested by D. P. Roux of the Reactor Controls Department of the Instrumentation and Controls Division. D. N. Fry of the Reactor Controls Department contributed extensively to this study by obtaining and reducing a large fraction of the experimental data. Useful discussions were had with Dr. Roux and Mr. Fry throughout the duration of this study.

---

*Summer participant and consultant from the Nuclear Engineering Department, University of Tennessee, Knoxville.

1. INTRODUCTION

Power spectral-density measurements have been used successfully[1,2] to obtain useful information from reactors operating at low power. Since such measurements do not perturb the system, they offer a technique for examining reactors operating at power to determine what useful information could be extracted from fluctuation of the neutron population. This technique was explored by a study of power spectral densities obtained from the ORR and the HFIR. For this study we made use of neutron fluctuation spectra obtained experimentally by others from the ORR at several power levels, flow rates, and control-rod positions,[3] and from the HFIR at several power levels and control-rod positions with different cores.[4]

To analyze and interpret the measured power spectral densities, we derived a distributed-parameter model to describe the dynamic behavior of the reactor. Calculated power spectral densities obtained using the distributed-parameter model were compared with those obtained using a lumped-parameter model.

Power spectra calculated using the distributed-parameter model were examined for different system parameters and driving functions to select the most likely combination of parameters and/or driving functions. The possible driving functions considered were:

1. statistical fluctuation of the fission density,
2. fluctuation of the coolant velocity,
3. fluctuation of the heat transfer coefficient,
4. fluctuation of the coolant temperature due to turbulence,
5. fluctuation of the inlet coolant temperature,
6. mechanical vibration of rods or fuel elements.

Hopefully, the model and study of experimental data described in this report will be helpful to others in similar studies of their reactor systems.

NOMENCLATURE

Φ_{00}	General power spectral density of the system output
Φ_{ii}	General power spectral density of the system input
Φ_{PP}^{obs}	Observed power spectral density of fluctuating current from a neutron-sensitive ionization chamber
$\Phi_{PP}^{chamber}$	Component of the observed power spectra due to the statistical nature of the neutron-detection process in the ionization chamber

---

[1] R. E. Uhrig, coordinator, *Noise Analysis in Nuclear Systems*, Proc. Symp. Univ. of Florida, Gainesville, Nov. 4–6, 1963, TID-7679.

[2] C. W. Ricker, S. H. Hanauer, and E. R. Mann, *Measurement of Reactor Fluctuation Spectra and Subcritical Reactivity*, ORNL-TM-1066 (April 1965).

[3] S. E. Stephenson, D. P. Roux, and D. N. Fry, *Neutron Fluctuation Spectra in the Oak Ridge Research Reactor*, ORNL-TM-1401 (May 1966).

[4] Personal communication from D. N. Fry, ORNL.

Φ_{PP}^{power}	Component of the observed power spectra due to fluctuation of the power (neutron-flux field)
Φ_{PP}^{NE}	Modified observed power spectra, experimental power spectral density, for fluctuation of the neutron-flux field
Φ_{PP}^{NC}	Calculated power spectral density for fluctuation of the neutron-flux field
Φ_{PP}^{PC}	Calculated power spectral density for fluctuation of the total power
$\Phi_{\rho\rho}$	Power spectral density for fluctuation of reactivity
ρ	Net reactivity
ρ_{ext}	Component of the net reactivity due to external (nonfeedback) effects
ρ_{int}	Component of the net reactivity due to feedback effects
G	Overall system-output-to-input transfer function
G_0	Zero-power transfer function
τ	Coolant transport time through the reactor core
h	Core length measured in the direction of flow
V	Velocity (speed) of the coolant in the core
α	Overall temperature coefficient of reactivity
α_c	Coolant temperature coefficient of reactivity
α_f	Fuel temperature coefficient of reactivity
δT	Variations in temperature about the mean
$\delta T_{j,eff}$	Fluctuations in the weighted volume average temperature for the coolant ($j = c$) or fuel ($j = f$)
P	Reactor power
δP	Variation in P about the operating level P_0
ω	Frequency in radians per second
S	Noise-equivalent source
s	Laplace and Fourier transform parameter
Λ	Neutron generation time
β_i	Effective delayed-neutron fraction for group i
β	$\sum_i \beta_i$
ϵ	Fraction of total neutron population absorbed by the detector
Q	Charge transferred per neutron absorbed
I_{DC}	dc component of ionization chamber current
$N(t)$	$P(t)/P_0$
$H(\mathbf{r})$	Spatial power density distribution
$H^*(\mathbf{r})$	Spatial importance distribution
$\rho_L(\mathbf{r},t)$	Local reactivity
$\Phi(\mathbf{r},t)$	Neutron flux
$C_i(\mathbf{r},t)$	The ith precursor density distribution

2. POWER SPECTRAL-DENSITY MODEL ANALYSIS

2.1 Introduction

Stephenson, Roux, and Fry[3] compared analytical and experimental power spectral densities for the ORR and concluded that fluctuation of the inlet coolant temperature is a possible explanation of the ORR spectra. In their analysis they used a lumped-parameter model whose applicability is questionable at high frequencies. They discussed this problem in their report and made recommendations to examine models which take into account distributed effects.

In this section, the expected frequency dependence on reactivity due to fluctuating inlet coolant temperature of constant amplitude at all frequencies is discussed qualitatively. Following this the analytical power spectral densities obtained from distributed- and lumped-parameter heat transfer models are compared quantitatively. Finally, the equations describing the model and the procedure for calculating the power spectral density for a specified (arbitrary) driving function are presented.

2.2 Expected Reactivity and Power Spectral Density Due to Inlet Temperature Fluctuation

The output power spectral density $\Phi_{00}(\omega)$ is related to the input power spectral density $\Phi_{ii}(\omega)$ by the expression[3]

$$\Phi_{00}(\omega) = |G(j\omega)|^2 \, \Phi_{ii}(\omega) \, , \tag{1}$$

where $G(j\omega)$ is the system frequency response function. A qualitative discussion of the expected output power spectral density for a simple input power spectral density follows for the case of a small light-water cooled and moderated power reactor with a negative temperature coefficient of reactivity.

It is assumed that fluctuation (assumed to be "white") of the inlet coolant temperature is the driving function for this system; that is, $\Phi_{ii}(\omega)$ is a constant. The fluctuation of the inlet coolant temperature does not affect the reactivity directly, but it is the propagation of these fluctuations up through the reactor core which introduces reactivity fluctuations. The propagation time τ is a function of the velocity V of the coolant and the length h of the core:

$$\tau = h/V \, . \tag{2}$$

For the special case in which the net gain of energy transferred to the coolant while traveling through the core is zero, the temperature distribution (relative to the mean temperature distribution) for the coolant can be synthesized for any specified frequency of fluctuation and time. For example, the axial temperature distributions (arbitrary units) for frequencies of periods 16τ, 4τ, 2τ, and τ are shown in Fig. 1. These temperature distributions are shown for the particular time at which the average temperature (over the core) is a maximum. In Fig. 2, the volume-average maximum temperature fluctuation is plotted as a function of the frequency of the inlet temperature fluctuation of magnitude ± 1.0 unit (arbitrary) for an h/V ratio of $\frac{1}{15}$ (for the ORR). Figure 2 is

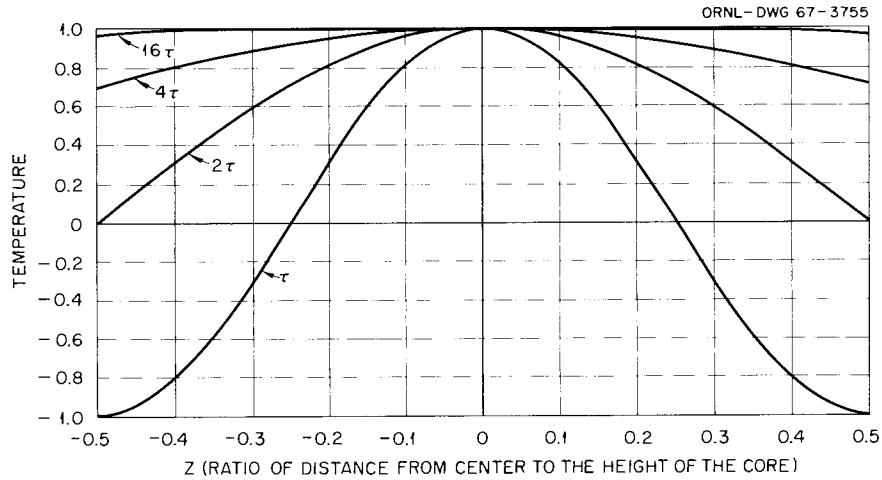

Fig. 1. Axial Temperature Distribution Relative to Same Reference Temperature for Various Periods τ of Oscillation at the Instant in Time When the Maximum Volume Average Temperature Will Occur.

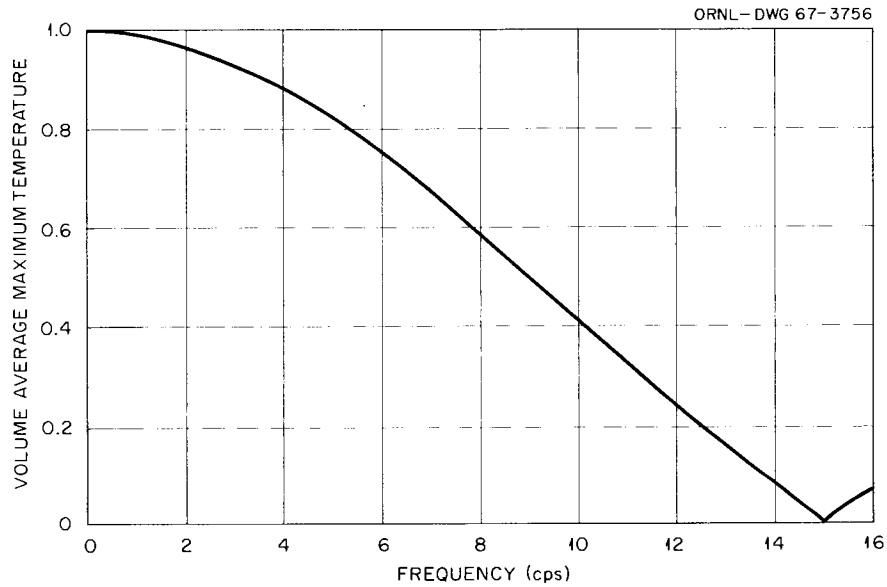

Fig. 2. Variation of the Maximum Volume Average Coolant Temperature with Frequency for a Ratio of $h:V$ of 1:15 and an Inlet Temperature Fluctuation of ±1.0 Unit.

interpreted as follows: with an inlet temperature variation between ±1.0 unit at 9 cps, then the volume-average temperature will fluctuate (at the same frequency) between ±0.5 unit; with an inlet temperature variation between ±1.0 unit at 15 cps, the volume-average temperature fluctuation will be zero.

Reactivity ρ introduced through fluctuations in temperature can be expressed as

$$\rho = \alpha \, \overline{\delta T} \, ,$$

where α is a temperature coefficient of reactivity and $\overline{\delta T}$ is some appropriate weighted temperature fluctuation. If there are fluctuations in the inlet coolant temperature, $\overline{\delta T}$ will be made up of two components in a power reactor: one due to the fluctuation of inlet temperature and one due to the fluctuation of power. In the following diagram of the system

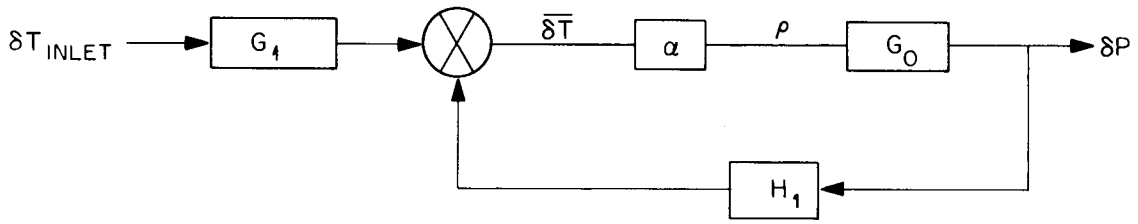

G_1, H_1, and G_0 are transfer functions; G_1 relates the average temperature fluctuation to the inlet temperature fluctuation, H_1 the average temperature fluctuation to the power fluctuation, and G_0 the power to reactivity (zero power); δP represents the power fluctuation. A single input-output system such as that illustrated can be described by

$$\delta P = G \, \delta T_{\text{inlet}} \, ,$$

where the composite transfer function G is given by

$$G = \frac{\alpha G_1 G_0}{1 + \alpha H_1 G_0} \, . \tag{3}$$

The output power spectral density $\Phi_{00}(\omega)$ of Eq. 1 is proportional to $|G|^2$ for a system with a driving function whose magnitude is independent of frequency; that is, $\Phi_{ii}(\omega)$ is independent of frequency. In particular, for a system with a white inlet temperature fluctuation, the modulus of Eq. 1 is given by Eq. 3; therefore, we can deduce the general behavior of $\Phi_{00}(\omega)$ with frequency from the discussion presented above. We commence by assuming that the break frequency of H_1 is low relative to that of G_1. The frequency dependence of the modulus of G_1 will be similar to that shown in Fig. 2; therefore, the break frequency of G_1 will be small relative to that for G_0 (in general). For negative feedback it follows that the modulus of G will possibly have a maximum over the frequency range between the break frequency of H_1 and the break frequency of G_1. The magnitude and sharpness of the "peak" in G depend on the characteristics of the system.

2.3 Comparison of Analytical Power Spectral Densities for Distributed- and Lumped-Parameter Models

In the frequency domain, the distributed-parameter model is described by a few coupled ordinary differential equations, whereas the lumped-parameter model is described by a set of

coupled algebraic equations. The validity of the distributed-parameter model is independent of the frequency. However, for a lumped-parameter model, an assumption must be made for the transient time for a given phenomenon, which necessarily leads to an upper limit for the frequency range for which the lumped-parameter model is valid. In principle, the upper frequency limit for the lumped-parameter model can be obtained as follows:

1. The equations describing the distributed-parameter model are expanded in a Taylor's series, from which the lumped-parameter model can be extracted.
2. From the preceding step, the error associated with the lumped-parameter model can be identified and determined as a function of frequency.

The difficulty with this procedure is that a great amount of labor is required to analyze a complicated system.

To generate a "feel" for the limitations of the distributed-parameter model, a simple example of a coolant flowing between and receiving energy from parallel plates was examined by use of both models (Appendix, Sect. 5.1). Comparison of the coolant temperature transfer functions for a lump of length h shows that both models give acceptable results provided that the inequality

$$h < V/\omega \tag{4}$$

is satisfied, where V is the average velocity of the coolant and ω is the frequency in radians per second. At frequencies up to 50 cps and a velocity of 30 fps (ORR conditions), the relationship $h < V/\omega$ states that h should be about 0.1 ft. This means that about 20 lumps would be required to model the ORR to obtain an acceptable calculated coolant temperature transfer function.

For a transfer function other than that discussed in the preceding paragraph, it does not follow that inequality (4) is applicable; however, due to the uncertainties associated with the validity of the lumped-parameter model, the distributed-parameter model was chosen for this study. Stephenson, Roux, and Fry[3] used the lumped-parameter model to calculate the square modulus of power to (1) the inlet-temperature frequency response function and (2) the reactivity frequency response function. Therefore, a comparison of the lumped- vs distributed-parameter model is available and presented here for completeness. The calculated square modulus of the power to the inlet-temperature frequency response as a function of frequency is presented in Fig. 3 for each model, and the calculated square modulus of the power to the reactivity frequency function is presented in Fig. 4 for each model. From Fig. 3, we conclude that the lumped-parameter model yields unacceptable results (for this study) for the modulus of the power to the inlet-temperature fluctuation frequency response function. In contrast, the modulus of the power to the reactivity frequency response function is independent of the model (see Fig. 4).

2.4 Calculation of Power Spectral Density

The HFIR and the ORR are assumed to be small systems neutronically; that is, any local perturbation in the flux field will perturb the entire field. Therefore a neutronic model that describes the volume-average behavior of the neutron field is sufficient, but for reactivity (temperature varia-

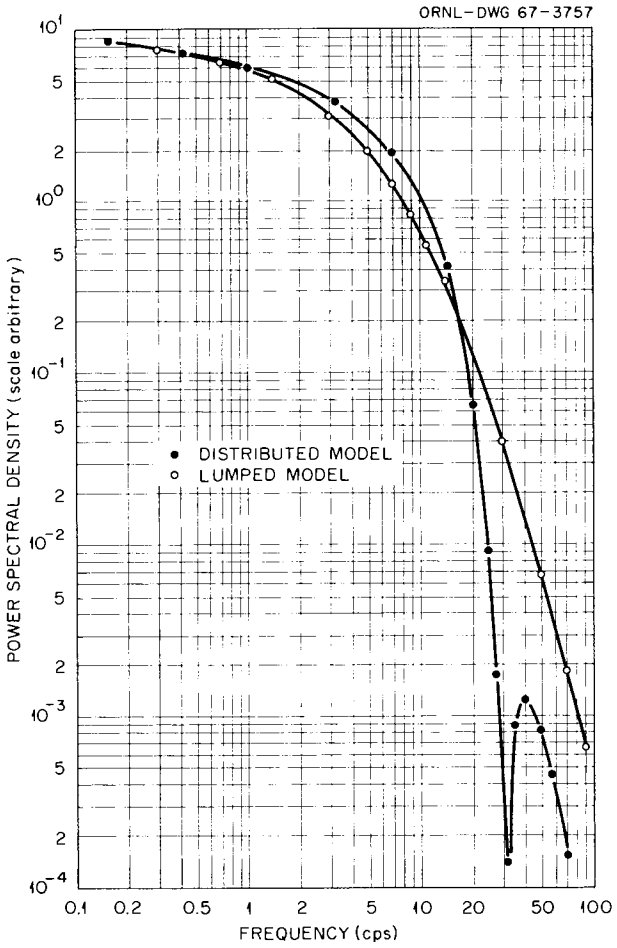

Fig. 3. Calculated Power Spectral Density for the ORR at 4.8 Mw and a Coolant Flow Rate of 18,000 gpm with an Inlet Coolant Temperature Driving Function.

tions, etc.) a model is required which will properly weight local perturbations. Therefore we started with the one-velocity diffusion equation and developed the point-model equation using the restricted variational principle.[5,6] As mentioned previously, the distributed-parameter model was used to describe the coolant and fuel temperatures. Since development of the linearized point-model equations in the frequency domain (with feedback) from the more basic models is lengthy (see Sect. 5.2), only the significant results are summarized here.

---

[5]D. E. Daugherty, *The Space-Time Neutron Kinetics by a Variational Method with Application to Power Reactor Dynamics*, KAPL-2217 (December 1962).

[6]J. C. Robinson, *Approximate Solution to the Time Dependent Multigroup Neutron Diffusion Equations Using a Restricted Variational Principle*, a dissertation presented to the graduate council of the University of Tennessee in partial fulfillment of the requirements for the degree of Doctor of Philosophy, December 1966.

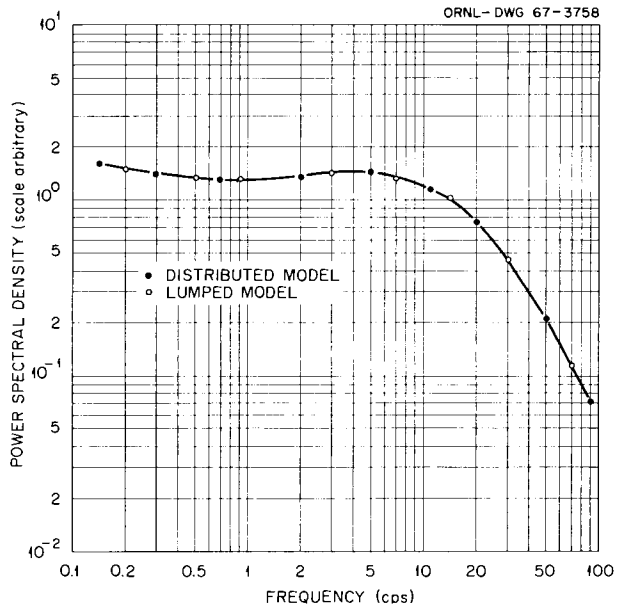

Fig. 4. Calculated Power Spectral Density for the ORR at 30 Mw with a Reactivity Driving Function.

The point-model equation for a power reactor (linearized model in the frequency domain) is

$$\left[\Lambda s + \beta - \sum_{i=1}^{6} \frac{\lambda_i \beta_i}{s + \lambda_i}\right] N(s) = \rho(s) \,, \tag{5}$$

where

$$\rho(s) = \sum_j \alpha_j \, \delta T_{j,\mathrm{eff}} + \rho_{\mathrm{ext}} \tag{6}$$

and

$$\delta T_{j,\mathrm{eff}} \equiv \frac{\int_r H^* \, \delta T_j(r, s) H \, dr}{\int_r H^* H \, dr} \,. \tag{7}$$

In Eq. 5, s is $j\omega$. In Eq. 6, ρ_{ext} takes into account external reactivities such as rod motion. In Eq. 7, $\delta T_j(r, s)$ is a function of the system parameters, power level, and the temperature boundary condition at the coolant inlet to the reactor. Equations 5 and 7 (see Appendix, Sect. 5.2) can be written as

$$\begin{bmatrix} \left(\Lambda s + \beta - \sum_{i=1}^{6} \frac{\lambda_i \beta_i}{s + \lambda_i}\right) & -\alpha_c & -\alpha_f \\ -B & D & 0 \\ -E & 0 & D \end{bmatrix} \begin{bmatrix} N \\ \delta T_{c,\mathrm{eff}} \\ \delta T_{f,\mathrm{eff}} \end{bmatrix} = \begin{bmatrix} \rho_{\mathrm{ext}} \\ A \, \delta T_{c,\mathrm{in}} \\ F \, \delta T_{c,\mathrm{in}} \end{bmatrix} \,, \tag{8}$$

where the coefficients A, B, E, and F are complex, D is a scalar, the subscripts c and f refer to the coolant and fuel respectively, and the subscript "in" refers to the upstream (inlet) end of the reactor core. Equation 8 was solved for $N(s)$, and the power spectral density was calculated from

$$\Phi_{PP}^{NC}(s) = N^*(s)\, N(s) \,. \tag{9}$$

In Eq. 9 the calculated power spectral density for the neutron fluctuations $\Phi_{PP}^{NC}(s)$ is related to the calculated power spectral density for the power fluctuations $\Phi_{PP}^{PC}(s)$ by

$$\Phi_{PP}^{NC}(s) = \frac{\Phi_{PP}^{PC}(s)}{P_0^2} \,, \tag{10}$$

since

$$P(s) = P_0 N(s) \tag{11}$$

for the assumed model.

3. COMPARISON OF ANALYTICAL WITH EXPERIMENTAL POWER SPECTRAL DENSITIES

3.1 Introduction

Most of the analytical results discussed in this section are for the ORR, because the model was specifically developed for this reactor; however, a few analytical results are presented for the HFIR. The model includes two temperature feedback paths, moderator and fuel, which adequately describe the ORR, but additional temperature feedback paths are required to describe the HFIR. Before a comparison of the results is given, equations that describe the calculated power spectral density and the observed power spectral density will be examined.

3.2 Presentation of Experimental Data

The calculated power spectral density (Eq. 9 or 10) is dimensionless, but the observed power spectral density from an ionization chamber has units and is affected by the detection efficiency, power level, and detection process itself. The objective of this section will be to determine a modified observed power spectral density that is equivalent to the calculated power spectral density $\Phi_{PP}^{NC}(s)$.

Before an expression for the observed power spectral density $\Phi_{PP}^{obs}(s)$ is introduced, Eq. 5 in the form

$$\left[\Lambda s + \beta - \sum_{i=1}^{6} \frac{\lambda_i \beta_i}{s + \lambda_i}\right] P(s) = P_0\, \rho(s) \tag{12}$$

will be examined, where $P(s)$ is given by Eq. 11 and P_0 is the reactor power level. For a reactor operating at very low power with no coolant flow, etc., the introduction of a noise-equivalent source[7] $S(s)$ will properly account for the statistical variations in the power level caused by the fission process. The inclusion of $S(s)$ in the model from which Eq. 12 was derived yields

$$\left[\Lambda s + \beta - \sum_{i=1}^{6} \frac{\lambda_i \beta_i}{s + \lambda_i}\right] P(s) = P_0\, \rho(s) + S(s) . \tag{13}$$

The zero-power reactivity transfer function $G_0(s)$ is given by

$$G_0(s) = \frac{1}{\left[\Lambda s + \beta - \sum_{i=1}^{6} (\lambda_i \beta_i / s + \lambda_i)\right]} ; \tag{14}$$

therefore Eq. 13 can be written as

$$P(s) = G_0(s)\, [P_0\, \rho(s) + S(s)] . \tag{15}$$

The power spectral density is obtained by multiplying Eq. 15 by its complex conjugate $P^*(s)$, which yields

$$\Phi_{PP}^{PC}(s) = |G_0(s)|^2 \{P_0^2\, \Phi_{\rho\rho}(s) + \Phi_{ss}(s) + P_0[\Phi_{\rho s}(s) + \Phi_{s\rho}(s)]\} . \tag{16}$$

If the fluctuation of reactivity is independent of the fluctuation of the noise-equivalent source, Eq. 16 reduces to

$$\Phi_{PP}^{PC}(s) = |G_0(s)|^2\, [P_0^2\, \Phi_{\rho\rho}(s) + \Phi_{ss}(s)] . \tag{17}$$

Cohn[7] has shown that the power spectral density of the noise-equivalent source is proportional to the power level; therefore, for a reactor operating at power, the second term on the right of Eq. 17 will be small, and hence Eq. 17 reduces to

$$\Phi_{PP}^{PC}(s) \cong |G_0(s)|^2\, P_0^2\, \Phi_{\rho\rho}(s) , \tag{18}$$

or from Eq. 10,

$$\Phi_{PP}^{NC}(s) = |G_0(s)|^2\, \Phi_{\rho\rho}(s) . \tag{19}$$

The function $\Phi_{PP}^{NC}(s)$ in Eq. 10 is equivalent to the function $\Phi_{PP}^{NC}(s)$ of Eq. 19.

Since the observed power spectral density for an ionization chamber consists of two parts,[7] one due to the statistical nature of the detection process and one due to fluctuation of the neutron

---

[7] C. E. Cohn, "A Simplified Theory of Pile Noise," *Nucl. Sci. Eng.* 7, 472–75 (1960).

field in the vicinity of the detector, the observed power spectral density can be expressed as

$$\Phi_{PP}^{obs}(s) = \Phi_{PP}^{chamber}(s) + \Phi_{PP}^{power}(s) . \tag{20}$$

The chamber power spectral density $\Phi_{PP}^{chamber}(s)$ is given by[7]

$$\Phi_{PP}^{chamber}(s) = \frac{2\epsilon Q^2 P_0}{\Lambda} , \tag{21}$$

where Q is the charge transferred per neutron absorbed, ϵ is the detection efficiency, and Λ is the neutron generation time. Since the second term of Eq. 20 is proportional to the calculated (or actual) power spectral density $\Phi_{PP}^{PC}(s)$, it can be written as

$$\Phi_{PP}^{power}(s) = \gamma \Phi_{PP}^{PC}(s) , \tag{22}$$

where γ, a proportionality constant that accounts for the process of observation, is given by[2,7]

$$\gamma = \frac{\epsilon^2 Q^2}{\Lambda^2} . \tag{23}$$

Equation 20 can now be written as

$$\Phi_{PP}^{obs}(s) = \frac{2\epsilon Q^2 P_0}{\Lambda} + \frac{\epsilon^2 Q^2}{\Lambda^2} \Phi_{PP}^{PC}(s) , \tag{24}$$

or

$$\Phi_{PP}^{obs}(s) = \frac{2\epsilon Q^2 P_0}{\Lambda} + \frac{\epsilon^2 Q^2 P_0^2}{\Lambda^2} \Phi_{PP}^{NC}(s) . \tag{25}$$

The average chamber current I_{DC} is[7]

$$I_{DC} = \frac{\epsilon Q P_0}{\Lambda} ;$$

therefore Eq. 25 becomes

$$\Phi_{PP}^{obs}(s) = 2QI_{DC} + I_{DC}^2 \Phi_{PP}^{NC}(s) . \tag{26}$$

We define an "experimental" power spectral density $\Phi_{PP}^{NE}(s)$ as

$$\Phi_{PP}^{NE}(s) \equiv \frac{[\Phi_{PP}^{obs}(s)/I_{DC}] - 2Q}{I_{DC}} . \tag{27}$$

From Eqs. 26 and 27, it is observed that

$$\Phi_{PP}^{NE}(s) = \Phi_{PP}^{NC}(s) . \tag{28}$$

In Eq. 27, $\Phi_{PP}^{obs}(s)$ and I_{DC} are observable, and $2Q$ is obtained from

$$\frac{\Phi_{PP}^{obs}(s)}{I_{DC}} = 2Q + I_{DC}\, \Phi_{PP}^{NC}(s) \tag{29}$$

at frequencies where $I_{DC}\, \Phi_{PP}^{NC}(s)$ is small relative to the constant $2Q$. The experimental power spectral-density data as determined by use of Eq. 27 will be displayed in the following sections.

3.3 Possible Driving Functions for the Power Spectra

Equation 28 states that the experimental and calculated power spectral densities are equal; however, it was assumed that the function $\Phi_{PP}^{PC}(s)$ used in the derivation of Eq. 28 was the actual or "true" power spectral density for the system. The functions $\Phi_{PP}^{NC}(s)$ (Eq. 9) and $\Phi_{PP}^{PC}(s)$ (Eq. 10) are determined by (1) the model, (2) the system parameters, and (3) the assumed driving function(s) (see Eq. 8). Since in this study the model was assumed to be correct, the problem was simplified to an examination of the calculated power spectra $\Phi_{PP}^{NC}(s)$ for different system parameters and driving functions. Then Eq. 28 was used to select the most likely combination of parameters and/or driving function(s). The possible driving functions considered in this study were

1. statistical fluctuation of the fission density,
2. fluctuation of the coolant velocity,
3. fluctuation of the heat transfer coefficient,
4. fluctuation of the coolant temperature due to turbulence,
5. fluctuation of the inlet coolant temperature,
6. mechanical vibration of rods or fuel elements.

Observed power spectra were obtained for the ORR[3] at various power levels and coolant flow rates. As will be shown, the experimental power spectral densities obtained from these observations are independent of the power level; therefore, statistical fluctuation of the fission density (see Eq. 17 and the preceding discussion) was eliminated as a possible driving function. A value of $\Phi_{PP}^{NC}(s)$ was determined for a 100% fluctuation in the magnitude of the heat transfer coefficient; since the value was a few orders of magnitude less than the magnitude of $\Phi_{PP}^{NE}(s)$, fluctuation of the film coefficient was eliminated as a possible driving function. With the assumption that fluctuation of the coolant temperature induced by turbulence was a driving function, it was calculated that the magnitude of these fluctuations must be about 0.3°F. However, a 0.3°F fluctuation due to turbulence is unreasonable, since a coolant temperature rise of approximately 11°F corresponds to 30 Mw of heat; therefore, fluctuation of the coolant temperature was not

considered to be a driving function. Evaluation of the fluctuation of the coolant velocity as a possible driving function was based on two considerations:

1. the effect of coolant velocity on the film coefficient and mass flow rate,
2. the possibility that a fluctuating coolant velocity could induce mechanical vibrations.

It is shown (in Sect. 5.2 and by Stephenson, Roux, and Fry[3]) that the effect of coolant velocity fluctuation on the film coefficient and mass flow rate will lead to a reactivity which is proportional to the power level. Since Stephenson, Roux, and Fry did not observe this effect during their experiments, this possible driving function was eliminated from further consideration. The second consideration, that a fluctuating coolant velocity could induce mechanical vibrations, has not been eliminated as a possible driving function.

Of the six driving functions considered, two (fluctuation of the inlet coolant temperature and vibration of rods or fuel elements) remain as possible driving functions.

The driving functions discussed thus far, when expressed as reactivity, are considered to be external driving functions. However, the total reactivity of a power reactor also includes feedback effects. Equation 19,

$$\Phi_{PP}^{NC}(s) = |G_0(s)|^2 \, \Phi_{\rho\rho}(s) \, , \tag{19}$$

is especially helpful in considering the effects of feedback on the power spectrum. In this equation, since $|G_0(s)|$ is the modulus of the zero-power reactor transfer function, $\Phi_{\rho\rho}(s)$ is the power spectrum for the total reactivity. The total reactivity ρ can be expressed as

$$\rho(s) = a_1 \, \rho_{ext}(s) + a_2 \, \rho_{int}(s) \, , \tag{30}$$

where the reactivity due to external effects is separated from the reactivity due to feedback (internal effects). From Eq. 30, $\Phi_{\rho\rho}(s)$ is constructed:

$$\Phi_{\rho\rho}(s) = \rho^*(s) \, \rho(s) \, ,$$

or

$$\Phi_{\rho\rho}(s) = a_1^2 \, \Phi_{11}(s) + a_1 a_2 [\Phi_{12}(s) + \Phi_{21}(s)] + a_2^2 \, \Phi_{22}(s) \, , \tag{31}$$

where

$$\begin{aligned} \Phi_{11}(s) &= \rho_{int}^*(s) \, \rho_{int}(s) \, , \\ \Phi_{12}(s) &= \rho_{int}^*(s) \, \rho_{ext}(s) \, , \\ \Phi_{21}(s) &= \rho_{ext}^*(s) \, \rho_{int}(s) \, , \\ \Phi_{22}(s) &= \rho_{ext}^*(s) \, \rho_{ext}(s) \, , \end{aligned} \tag{32}$$

and a_1 and a_2 are coefficients of combination. The second and third terms of Eq. 31 depend on

the reactor power level; therefore, for a constant external reactivity, the effects of feedback on the power spectra can be examined explicitly by observing the power spectra at various power levels.

3.4 Power Spectral Density for the ORR

The values of $\Phi_{PP}^{NE}(s)$ for the ORR[3] are plotted in Fig. 5 for various power levels and in Fig. 6 for different coolant flow rates. The values of $\Phi_{PP}^{NC}(s)$ (Eq. 9) for the ORR are plotted in Figs. 7 through 9:

1. Figure 7 is a plot of $\Phi_{PP}^{NC}(s)$ as a function of a white (amplitude independent of frequency) reactivity ρ driving function of unit magnitude at reactor power levels of 4.8 and 30 Mw.
2. Figure 8 is a plot of $\Phi_{PP}^{NC}(s)$ as a function of inlet coolant temperature fluctuations of 1°F, coolant velocity of 18,000 gpm, and power levels of 4.8 and 30 Mw.
3. Figure 9 is a plot of $\Phi_{PP}^{NC}(s)$ as a function of inlet coolant temperature fluctuations of 1°F, a power level of 4.8 Mw, and coolant flow velocities of 4500, 9000, and 18,000 gpm.

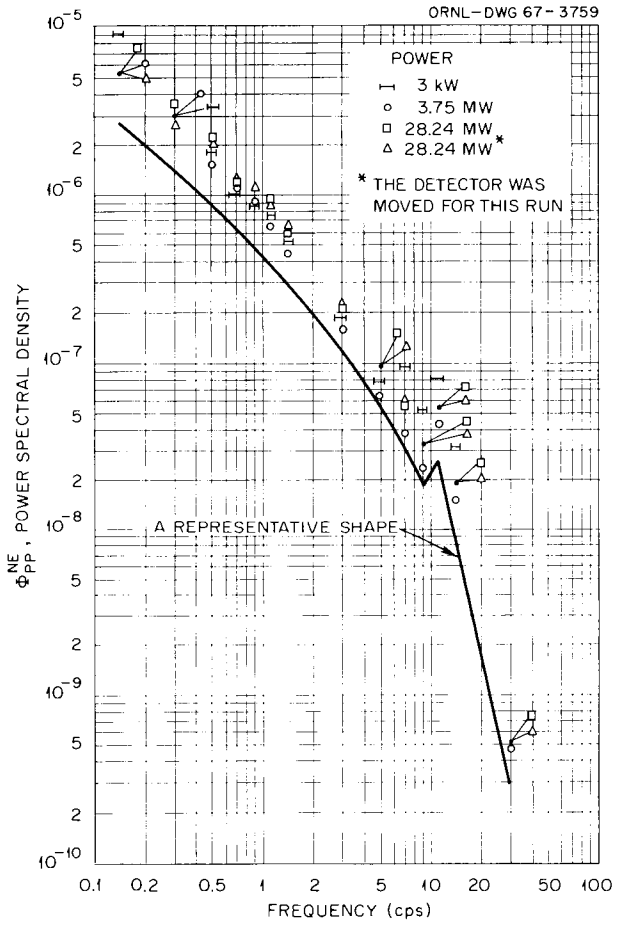

Fig. 5. Experimental Power Spectra for the ORR at Different Power Levels and a Coolant Flow Rate of 18,500 gpm.

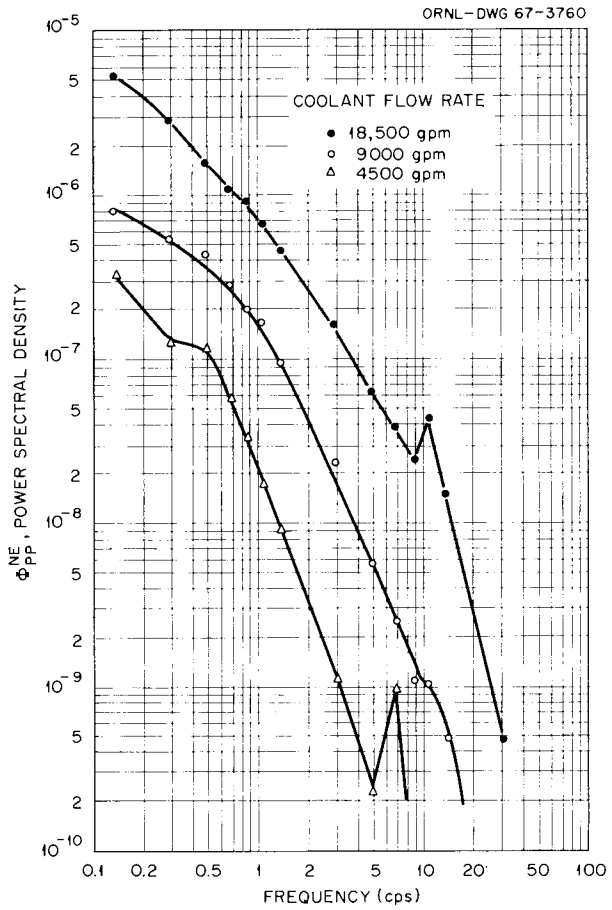

Fig. 6. Experimental Power Spectra for the ORR at Different Coolant Flow Rates and 3.75 Mw.

When the function $\Phi_{PP}^{NC}(s)$ as given by Eq. 19 was discussed in Sect. 3.3, it was explained that the reactivity spectral density $\Phi_{\rho\rho}(s)$ would be affected by the power level because of increased feedback with power. Figures 7 and 8 show that the effect of feedback on the function $\Phi_{PP}^{NC}(s)$ is very small over the frequency range of observation. This conclusion is verified conclusively by the lack of effect of $\Phi_{PP}^{NE}(s)$ in Fig. 5; therefore, $\Phi_{PP}^{NE}(s)$ is essentially the product of the square of the modulus of the zero-power transfer function $|G_0(s)|^2$ and the power spectra of the external reactivity. The function $\Phi_{PP}^{NC}(s)$ of Fig. 8 is essentially $|G_0(s)|^2$, because a value of unity was used for $\Phi_{\rho\rho}(s)$. From the magnitudes of $\Phi_{PP}^{NE}(s)$ of Fig. 5 and $\Phi_{PP}^{NC}(s)$ of Fig. 7, the magnitude of the external reactivity ρ_{ext} can be obtained at any desired frequency; for example, at 0.1 cps,

$$\rho_{ext} = \left[\frac{\Phi_{PP}^{NE}(0.1)}{|G_0(0.1)|^2}\right]^{1/2}$$

$$\simeq 10^{-3}\% .$$

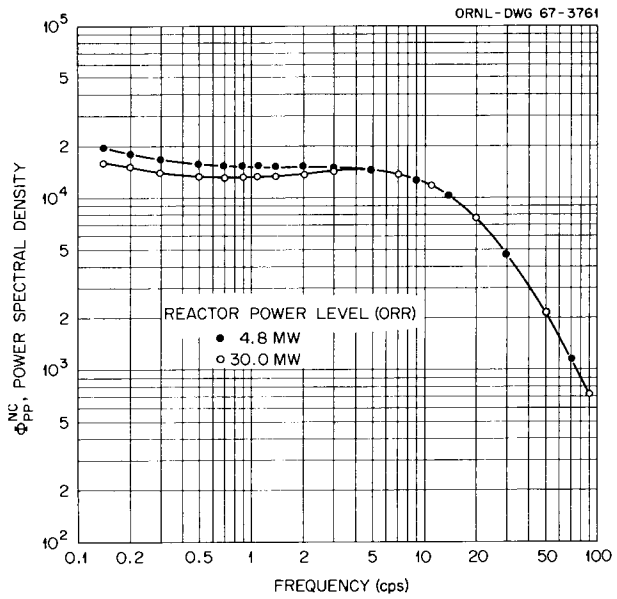

Fig. 7. Calculated Power Spectral Density for the ORR at 4.8 and 30 Mw with a White Reactivity Driving Function of Unity Magnitude.

Comparison of the magnitude of spectral densities in Fig. 5 with Fig. 7 shows that if fluctuation of the inlet coolant temperature is the driving function, then a fluctuation of about 0.5°F is required at a frequency of 0.1 cps.

In Fig. 6 it is evident that the magnitude and frequency of the external driving function are dependent on the coolant flow rate. The calculated power spectral densities for a white fluctuation of inlet temperature at different flow rates are presented in Fig. 9. At a low flow rate of 4500 gpm, a 0.07°F fluctuation of the inlet coolant temperature at 0.1 cps is required to explain the magnitude of $\Phi_{PP}^{NE}(s)$.

The required magnitude of the temperature fluctuation coupled with the required frequency dependence on the coolant flow rate appear to be physically unreasonable. Furthermore, if the detailed structure of $\Phi_{PP}^{NE}(s)$ in Fig. 6 is to be explained by a driving function due to inlet temperature fluctuation, then the spectral density of the inlet temperature fluctuation must exhibit resonances.

Because these requirements of magnitude and frequency dependence are unreasonable, we conclude that the inlet temperature fluctuation is not the primary driving function.

This conclusion leaves only mechanical vibration of the rods or fuel elements as a primary driving function. A mechanism that could cause such mechanical vibration is fluctuation of the coolant velocity. Figure 6 shows that the driving function is strongly related to the average flow rate. Power spectral-density spectra reported[8] for the Hitachi Training Reactor (HTR) for power

[8]S. Yamada and H. Kage, "Reactor Noise Caused by Coolant Flow Fluctuation," pp. 455–62 in *Proc. Symp. Neutron Noise, Waves, and Pulse Propogation*, AEC Symposium Series No. 9, University of Florida, Gainesville, Feb. 14–16, 1966.

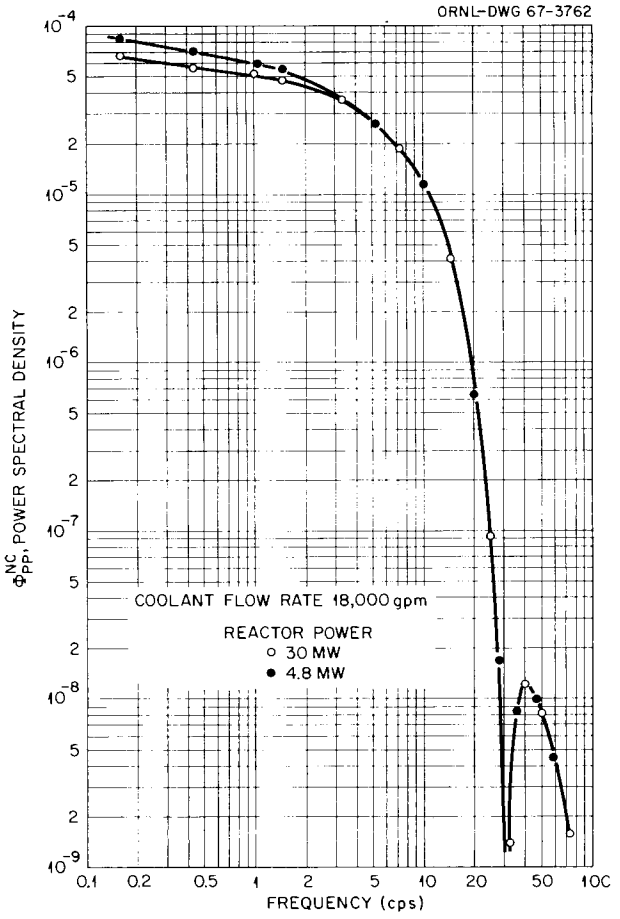

Fig. 8. Calculated Power Spectral Density for the ORR for Inlet Temperature Fluctuations of 1°F at Different Power Levels.

and coolant fluctuations show strong correlation between the power and coolant spectral densities, which suggests that rod vibrations are induced by coolant fluctuations.

No attempt was made in this study to construct a model for mechanical vibrations due to fluctuations in the coolant velocity; however, insight can be acquired for the expected power spectral density for mechanical motion by examining a simple resonant system whose displacement $x(t)$ is related to a driving function $z(t)$ by

$$\frac{d^2x(t)}{dt^2} + 2\zeta\omega_0 \frac{dx(t)}{dt} + \omega_0^2\, x(t) = z(t)\ , \tag{33}$$

where ζ is usually referred to as the system damping constant. The power spectral density for the output $\Phi_{xx}(\omega)$ is related to the power spectral density for the input $\Phi_{zz}(\omega)$ by

$$\Phi_{xx}(\omega) = |G(\omega)|^2\, \Phi_{zz}(\omega)\ , \tag{34}$$

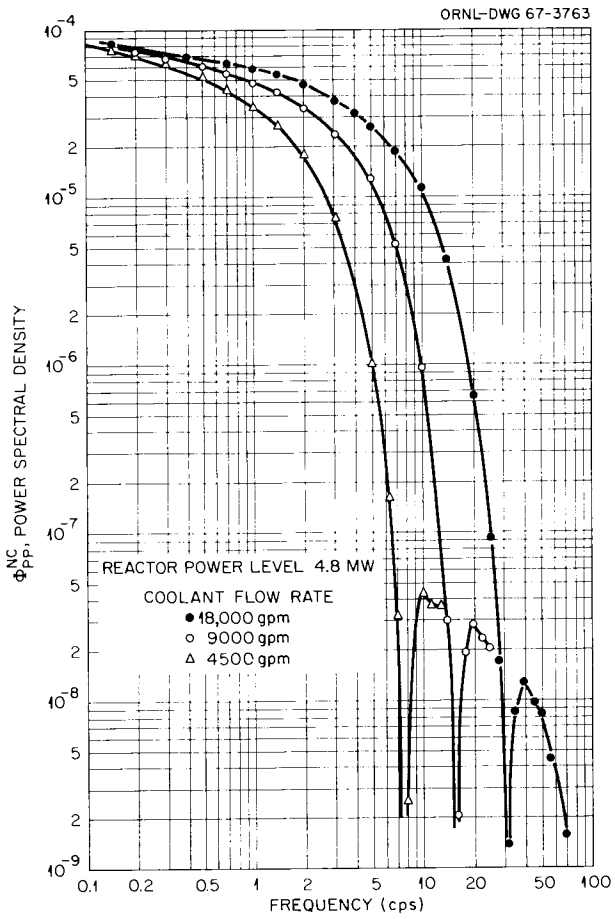

Fig. 9. Calculated Power Spectral Density for the ORR at 4.8 Mw for a White Inlet Temperature Fluctuation Driving Function.

where $|G(\omega)|^2$ is given by[9]

$$|G(\omega)|^2 = \frac{1}{\omega_0^2\{[1-(\omega/\omega_0)^2]^2 + [2\zeta(\omega/\omega_0)]^2\}}. \tag{35}$$

From Eq. 35, $|G(0)|^2$ is determined to be ω_0^{-2}, which is a possible maximum; however, if the inequality

$$[1-(\omega/\omega_0)^2]^2 + [2\zeta(\omega/\omega_0)]^2 < 1 \tag{36}$$

is satisfied for some frequency ω greater than zero, then $|G(\omega)|^2$ will have a maximum for some

[9] J. A. Thie, *Reactor Noise*, Rowman and Littlefield, New York, 1963.

frequency ω – say ω_{max}. From inequality 36, an ω_{max} greater than zero exists if

$$(1 - 2\zeta^2) > 0 \; ; \tag{37}$$

that is, an ω_{max} exists if the system damping constant squared ζ^2 is less than 0.5. If inequality 37 is satisfied, ω_{max} is (from Eq. 35)

$$\omega_{max} = \omega_0 [1 - 2\zeta^2]^{1/2} \tag{38a}$$

for $\zeta^2 < 0.5$ (or $\zeta < 0.707$), and

$$\omega_{max} = 0 \tag{38b}$$

for $\zeta \geq 0.707$. Positive values are chosen for ζ, because negative values imply a nonstationary system, as can be deduced from the roots $\Gamma_{1,2}$ of Eq. 33; that is,

$$\Gamma_{1,2} = -\omega_0 \zeta \pm j\omega_0 [1 - \zeta^2]^{1/2} \; . \tag{39}$$

From Eqs. 38 and 39, it is seen that the maximum value of $|G(0)|^2$ (Eq. 35) will shift from a frequency of ω_0 for an undamped system with $\zeta = 0$ to a frequency of zero for a damped system with $\zeta > 0.707$.

A further property of Eq. 35 can be obtained by considering values of $(\omega/\omega_0)^2$ larger than unity; then Eq. 35 can be written as

$$|G(\omega)|^2 \cong \frac{1}{\omega_0^2 (\omega/\omega_0)^2 [(\omega/\omega_0)^2 + 2\zeta]} \; . \tag{40}$$

Furthermore, for $(\omega/\omega_0)^2 >> 2\zeta$, Eq. 40 becomes

$$|G(\omega)|^2 \cong \frac{\omega_0^2}{\omega^4} \; . \tag{41}$$

Therefore, if the displacement $x(t)$ of Eq. 33 represents rod or fuel-element motion, and it is further postulated that the driving function $z(t)$ is white, then the power spectra for the rod motion would vary as dictated by Eq. 41 for large values of ω relative to ω_0.

Further examination of Eq. 35 shows that $|G(\omega)|^2 \to \infty$ at $\omega = \omega_0$ as $\zeta \to 0$. Also, for values of $0 < \zeta < 0.707$, $|G(\omega)|^2$ is reasonably constant (slowly increasing) for frequencies such that $\omega/\omega_{max} < 0.8$.

When rod and fuel-element vibrations are considered which are assumed to exist due to fluctuations in the coolant velocity, it follows that the net system reactivity caused by these vibrations may be made up of two correlated components. Therefore, the spectral-density function for the net reactivity would be given by an expression analogous to Eq. 31. To determine how two correlated reactivity driving functions might affect the neutron power spectral-density function,

calculations were performed for an assumed white reactivity ρ and a white inlet temperature fluctuation. It was arbitrarily assumed that the reactivity would lead the inlet temperature fluctuations by a fixed (specified) angle at all frequencies. This particular scheme was chosen because it was simple to modify the computer code which had previously been implemented to solve the equations of the model. The results for these assumed correlated driving functions are shown in Figs. 10 and 11. The significant points to be noted in Figs. 10 and 11 are as follows:

1. The reactivity is the dominant driving function for frequencies above about 20 cps.
2. At frequencies below 5 to 10 cps, the temperature fluctuation is usually the dominant driving function.
3. In the "transition" region of 5 to 20 cps, the shape of the power spectral density is strongly dependent on (1) the relative magnitude of the assumed driving functions and (2) the assumed correlation of the two driving functions.

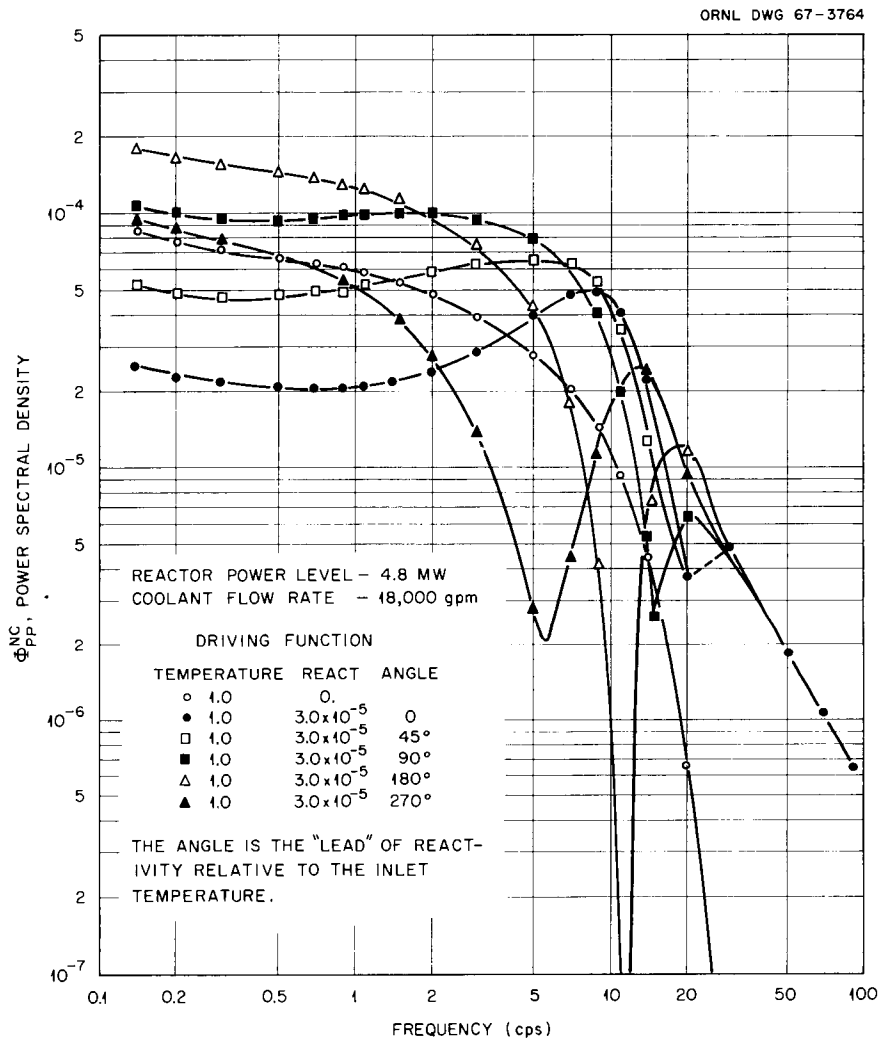

Fig. 10. Calculated Power Spectral Density for an Assumed "Correlated" Driving Function of Inlet Temperature and Reactivity Fluctuation.

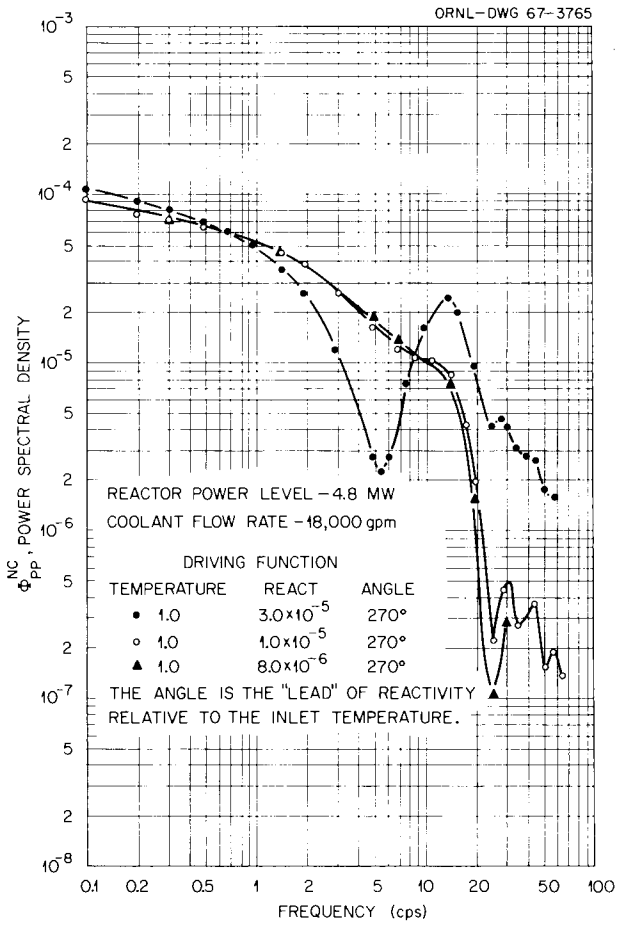

Fig. 11. Calculated Power Spectral Density for a Specified Correlation Between Reactivity and Inlet Temperature.

The ORR data in Fig. 5 were obtained for control rod positions at about 16.5 in. If vibration of the control rods is a significant driving function, then the power spectra obtained during the life of the core (at different rod positions) should vary. Fry[10] obtained power spectral-density data for the ORR at various rod positions; a few are presented in Figs. 12 and 13.

A comparison of the power spectral densities of Fig. 5 with those of Fig. 12 reveals that the peak at 11 cps in Fig. 5 is not present in Fig. 12; however, there is a peak at 5 cps. Tabor and Hurt[11] state that it was necessary to replace "the south upper-shim-rod bearing (hold-down arm)" to reduce shim-rod vibrations. This rod-bearing replacement occurred during the interval of time which elapsed between the collection of data reported by Stephenson, Roux, and Fry[3]

[10] Personal communication from D. N. Fry, ORNL, in regard to the experimental power spectral-density data for the ORR, 1967.

[11] W. H. Tabor and S. S. Hurt III, *Oak Ridge Research Reactor Quarterly Report October, November, and December of 1965*, ORNL-TM-1503 (April 1966).

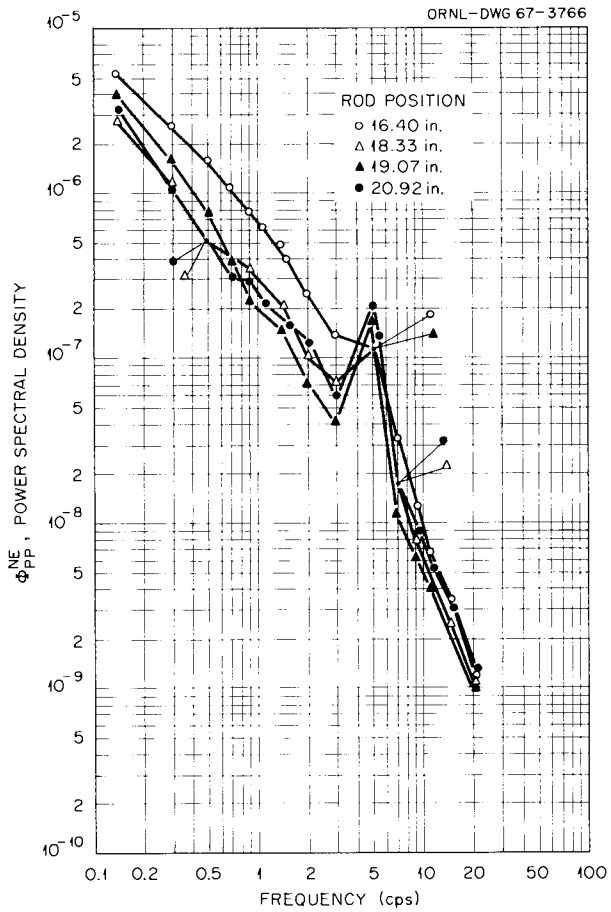

Fig. 12. Experimental Power Spectral Density for the ORR at 30 Mw and Different Control-Rod Positions.

and that obtained by Fry.[10] Therefore, it is concluded that the peak in the spectrum is due to rod vibration.

A comparison of Figs. 12 and 13 reveals the same general behavior in both instances for the power spectral density in response to rod position except that the amplitude in Fig. 13 is less. Basically, the data in Figs. 12 and 13 are for the same core; however, the reactor was shut down and the fuel elements were rearranged in the time interval between the collection of data shown in Figs. 12 and 13. Therefore, from these data it appears that fuel element vibrations contribute to the observed neutronic noise.

Although, in general, the amplitude of the power spectral density decreases as the control rods are withdrawn from the core, the magnitude of the peak increases as the rods are withdrawn (see Figs. 12 and 13). Physically, when the rods are withdrawn, they are pushed from the core into the inlet flow plenum.

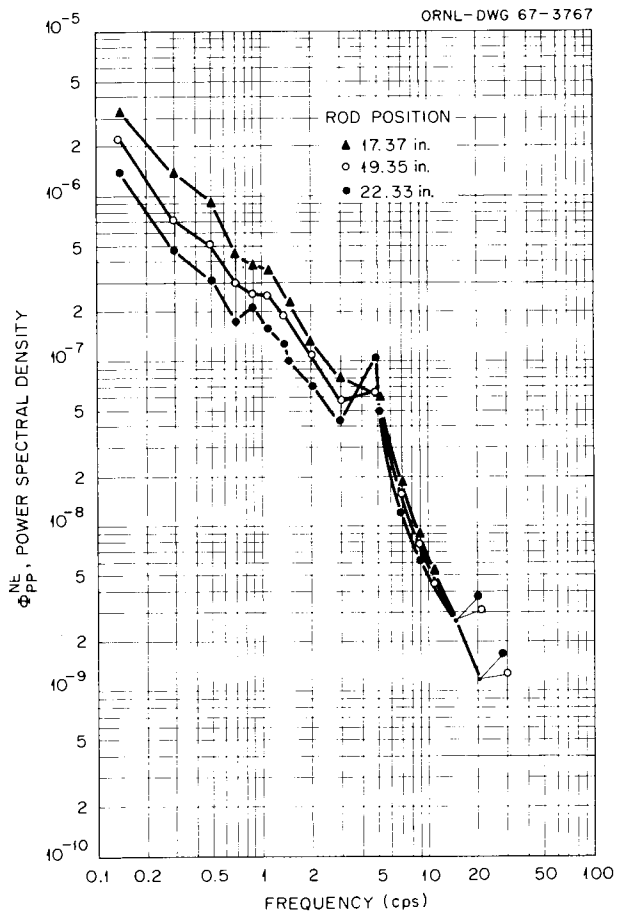

Fig. 13. Experimental Power Spectral Density for the ORR at 30 Mw and Different Control-Rod Positions.

3.5 Power Spectral Density for the HFIR

Many spectral measurements were obtained for the HFIR by Fry.[12] The calculated spectrum due to a white inlet-temperature fluctuation of 0.1°F is shown in Fig. 14 for two power levels. The coolant velocity is higher in the HFIR than in the ORR, which accounts for the higher roll-off frequency. Since the neutron generation time in the HFIR is expected to increase (approximately double) during the life of the core, a calculation was made to determine what effect this would have on the spectra. Figure 15 shows the effects of lifetime variation and feedback, but the feedback effects in Figs. 14 and 15 are probably too large since the effects of the target and control rod coolants, which have positive temperature coefficients,[13] were not taken into

[12] D. N. Fry, *Neutron Density Fluctuation Analysis as a Reactor Diagnostic Tool at the HFIR*, ORNL-TM-1871 (to be published).

[13] B. R. Lawrence, *Determination of the Power Reactivity Frequency Response Function of a Power Reactor with Application to the High Flux Isotope Reactor*, ORNL-TM-1471 (July 1966).

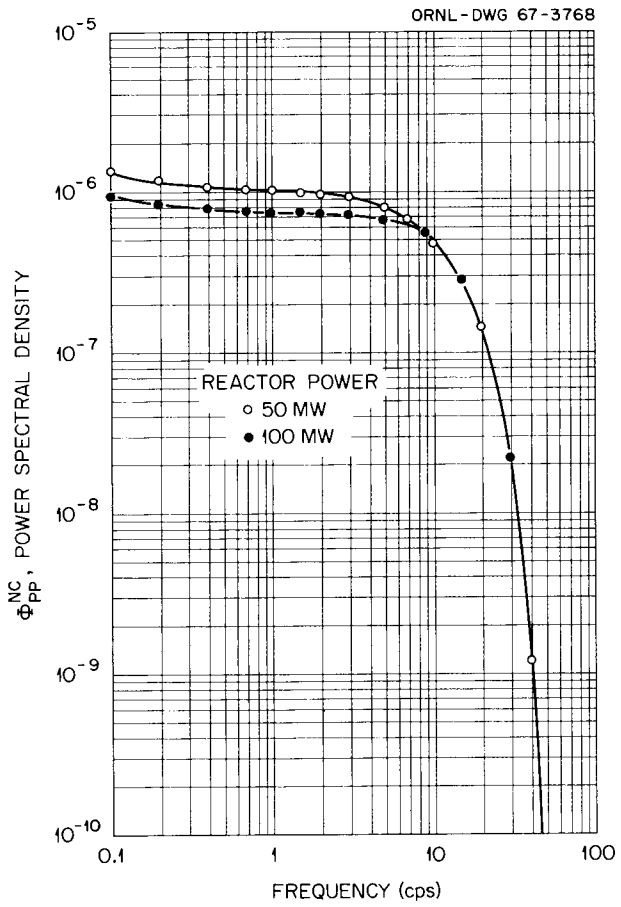

Fig. 14. Calculated Power Spectral Density for the HFIR for a White Inlet Temperature Fluctuation of 0.1°F and a Fuel Channel Coolant Velocity of 51 fps.

account. The change in generation time had very little effect on the power spectra at frequencies below 15 cps.

Significant features of spectra (Fig. 16) obtained during an approach to full power (approximately 100 Mw) are that (1) there is a broad peak at 1 to 2 cps which decreases with power, and (2) the spectra increases with power at frequencies below 0.2 cps. Figures 16 and 17 show the observed spectra for the same core during its life, that is, with the control rods withdrawn. The significant features in Fig. 17 are as follows:

1. A broad peak in the range from 1 to 2 cps for the approach to full power shifts to lower frequencies as the rods are withdrawn.
2. The magnitude of the spectrum decreases significantly above 1 cps except for the last 1.5 in. of rod movement.
3. There is a peak at 20 cps for a rod position of 21.18 in.
4. There is a peak which begins at 5 cps for a rod position of 23.53 in. and is higher at a rod position of 25.00 in.

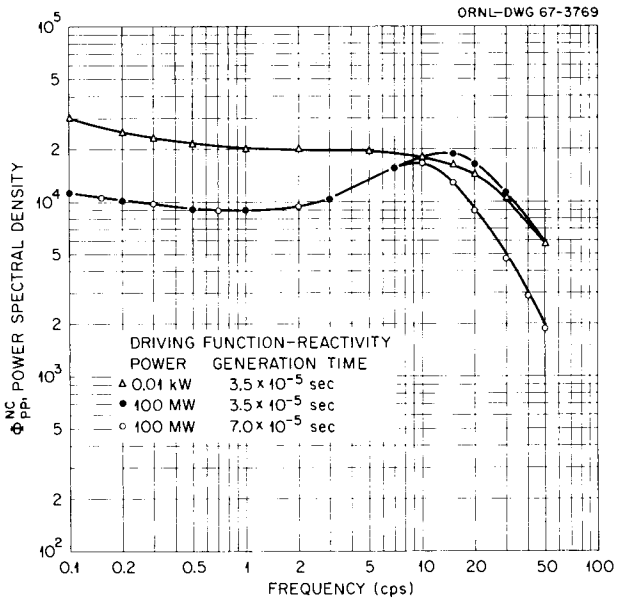

Fig. 15. Calculated Power Spectral Density for the HFIR with a Reactivity Driving Function of Unity Magnitude.

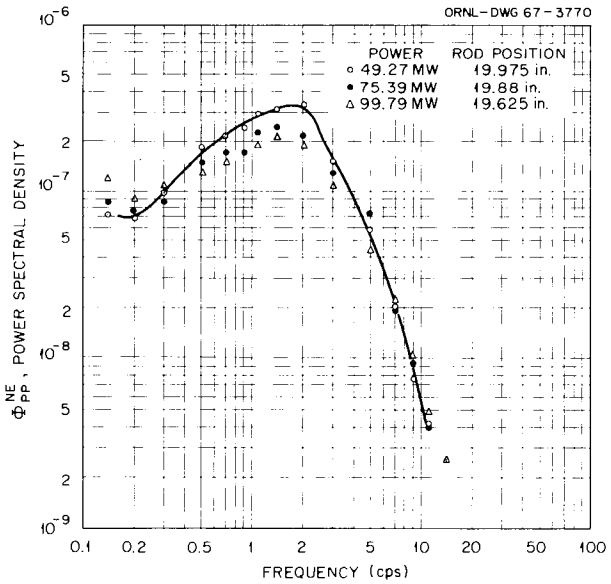

Fig. 16. Experimental Power Spectral Density for the HFIR at Various Power Levels.

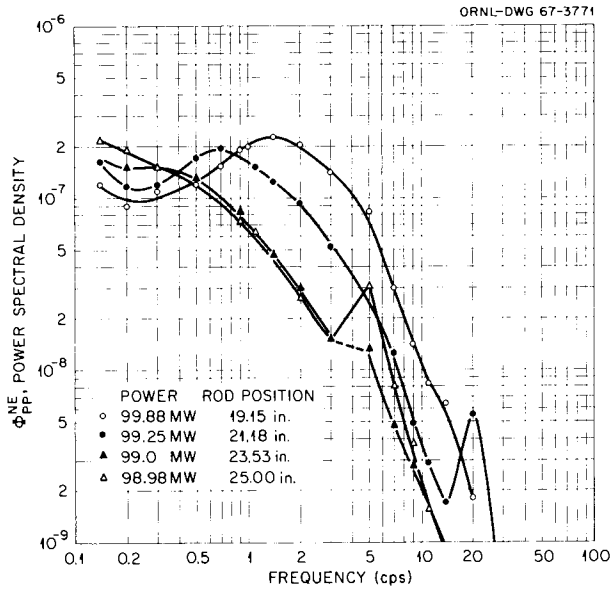

Fig. 17. Experimental Power Spectral Density for the HFIR at Various Rod Positions.

Over the frequency range of 0.1 to 10 cps in Figs. 14 and 15, the calculated power spectral density is reasonably flat for an assumed white inlet-temperature fluctuation or rod vibration. Furthermore, a change in lifetime has no effect on the calculated power spectra in this frequency range. Therefore the shape of the observed spectra (see Figs. 16 and 17) is essentially due to the spectral density of the external reactivity driving function such as mechanical (rod) vibrations or temperature fluctuations.

Figure 16 shows that the power spectra decreased, in general, with power in the frequency range from 0.4 to 7 cps. This can be partially explained by feedback effects (see Fig. 13), but it is also evident that the spectra increased with power below 0.4 cps, which is contrary to what one would expect if feedback were significant. However, if the temperature fluctuates, then the magnitude of the fluctuation might increase with power. An assumption that the fluctuation decreases with frequency (this is physically reasonable) would explain the effect at the low frequencies. The magnitude of temperature variation required for the power fluctuations observed at 0.14 cps in Fig. 16 would be about 0.03 to 0.05°F.

Since the peak at 20 cps in Fig. 17 has been observed at about this same rod position for cores previously studied, we conclude that this peak is due to rod oscillation. However, finer resolution is required to state conclusively that the peak is at 20 cps. The peak at 5 cps had not been observed before; therefore, it was inferred that the rods are vibrating excessively at this frequency. Shortly after the run in which these data were taken with a rod position of 25.0 in., a defective rod bearing was detected. After the bearing was replaced the peak did not appear in data obtained for subsequent runs. Thus, we conclude that excessive rod vibration was the cause of the 5-cps peak.

4. CONCLUSIONS

The difference between the lumped- and the distributed-parameter model increased as the frequency increased. For an upper frequency limit of 30 cps, acceptable results were calculated from the lumped-parameter model (a single lump) for the ORR and the HFIR for a uniform insertion of reactivity driving function; however, acceptable results were not obtained from the lumped-parameter model for an inlet coolant temperature fluctuation. Since digital machines are generally employed, we recommend that a distributed-parameter model be used.

The $\Phi_{PP}^{NE}(s)$ is independent of power level or detector efficiency (Eq. 27) when internal feedback effects on reactivity are insignificant (Eq. 31). Further, since feedback effects were small for the ORR and the HFIR over the frequency range 0.1 to 30 cps, we conclude that the power spectral-density measurement at power is a measure of the external reactivity spectral density.

For the ORR the fluctuating coolant temperature did not contribute significantly to the observed spectral density, and the driving function is the vibration of control rods and perhaps the vibration of fuel elements.

For the HFIR the dominant driving function is rod vibration for rod positions less than about 23.0 in. For rod positions numerically larger than 23.0 in., it is possible that temperature fluctuation or some other mechanism (such as vibration of the central target) contributed to the total external reactivity.

Since the power spectra for the ORR or the HFIR did not exhibit significant power dependence, it would be useless to attempt any parameter extraction (such as temperature coefficient of reactivity) from the observed spectra; therefore, no attempt was made to do so.

5. APPENDIX

5.1 Comments on Maximum Nodal Size for a Lumped-Parameter Model

The objective of this section will be to develop a criterion for selecting a minimum number of nodes which must be included in a lumped-parameter model for the calculation of a physically acceptable frequency response function. In particular, attention will be focused on a stationary-fueled reactor in which the energy is transported from the reactor to an external sink by a coolant that can be adequately described with one-dimensional flow. Then, a solution for a single node for the exit temperature will be obtained using the lumped- and distributed-parameter models. These solutions will be compared at various frequencies and appropriate conclusions presented.

Suppose that energy is transported to the coolant by conduction as shown in Fig. 18. Take the equation describing the temperature of the coolant in the axial direction (z direction) to be

$$\frac{\partial T_c}{\partial t} + V \frac{\partial T_c}{\partial z} = B(T_w - T_c) , \tag{42}$$

where T_c is the coolant temperature, T_w is the wall temperature, and B is a constant.

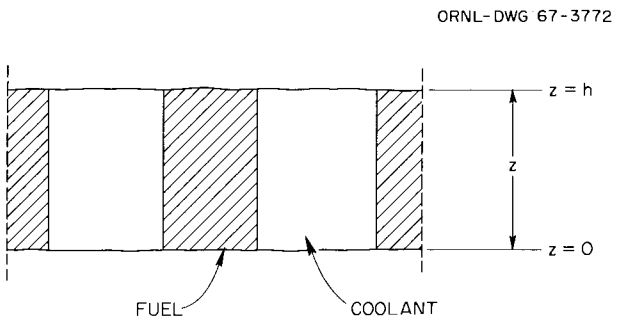

Fig. 18. Arrangement of Fuel and Coolant.

The objective is to calculate a frequency response function for a variation in T_c at $z = h$ by the lumped- and distributed-parameter technique. For simplicity, T_w will be assumed constant. The temperature at $z = 0$ will be assumed to be varying with time in some prescribed fashion.

Replace T_c and T_w in Eq. 42 with

$$T_c(z, t) = T_c(z, 0) + T_c'(z, t)$$

and

$$T_w(z, t) = T_w(z, 0) ,$$

which leads to

$$\frac{\partial T_c'}{\partial t} + V \frac{\partial T_c'}{\partial z} = -BT_c' , \tag{43}$$

since (at steady state)

$$V \frac{\partial T_c(z, 0)}{\partial z} = B[T_w(z, 0) - T_c(z, 0)] . \tag{44}$$

We first solve Eq. 43 by the distributed-parameter technique; that is, we transform Eq. 42 and integrate with respect to z. The result is (dropping primes)

$$T_c(h, s) = e^{-(s+B)h/V} T_c(0, s) . \tag{45}$$

For the lumped-parameter model, we integrate Eq. 42 over z, introduce approximations, and then transform the resultant equations. This sequence is presented below:

1. Integrate over z to obtain

$$\int_0^h \frac{\partial T_c}{\partial t} dz + V \int_0^h \frac{\partial T_c}{\partial z} dz = -B \int_0^h T_c \, dz . \tag{46}$$

2. Introduce the approximations

$$\int_0^h \frac{\partial T_c}{\partial t}\, dz \approx \frac{d}{dt}\left\{\frac{1}{2}\left[T_c(h,\ t) + T_c(0,\ t)\right]\right\} h\ ,$$

$$\int_0^h \frac{\partial T_c}{\partial z}\, dz \approx \frac{T_c(h,\ t) - T_c(0,\ t)}{h}\ h\ ,$$

$$\int_0^h T_c\, dz \approx \frac{1}{2}\left[T_c(h,\ t) + T_c(0,\ t)\right] h\ .$$

Then Eq. 46 becomes

$$\frac{d}{dt}\left[T_c(h,\ t) + T_c(0,\ t)\right] + \left[\frac{2V}{h} + B\right] T_c(h,\ t) = \left[\frac{2V}{h} - B\right] T_c(0,\ t)\ . \tag{47}$$

3. Transform Eq. 47 to obtain

$$T_c(h,\ s) = \frac{[(2V/h) - B] - s}{[(2V/h) + B] + s}\ T_c(0,\ s)\ . \tag{48}$$

Replace s by $j\omega$ in Eqs. 45 and 48 and write the resultant equations in the form

$$T_c(h,\ j\omega) = e^{-(hB/V)}\ e^{-j(h\omega/V)}\ T_c(0,\ j\omega)\ , \tag{49}$$

$$T_c(h,\ j\omega) = \frac{[2 - (hB/V)] - j(h\omega/V)}{[2 + (hB/V)] + j(h\omega/V)}\ T_c(0,\ j\omega)\ . \tag{50}$$

Separating Eq. 49 into components leads to

$$\mathrm{Re}\left[\frac{T_c(h,\ j\omega)}{T_c(0,\ j\omega)}\right] = e^{-(hB/V)} \cos\frac{h\omega}{V}\ , \tag{51a}$$

$$\mathrm{Im}\left[\frac{T_c(h,\ j\omega)}{T_c(0,\ j\omega)}\right] = -\,e^{-(hB/V)} \sin\frac{h\omega}{V}\ ; \tag{51b}$$

and Eq. 50 yields

$$\mathrm{Re}\left[\frac{T_c(h,\ j\omega)}{T_c(0,\ j\omega)}\right] = \frac{[2 - (hB/V)][2 + (hB/V)] - (h\omega/V)^2}{[2 + (hB/V)]^2 + [(h\omega/V)]^2}\ , \tag{52a}$$

$$\mathrm{Im}\left[\frac{T_c(h,\ j\omega)}{T_c(0,\ j\omega)}\right] = -4\ \frac{h\omega/V}{[2 + (hB/V)]^2 + [(h\omega/V)]^2}\ . \tag{52b}$$

Equations 51 and 52 can be expanded (for comparison) for the special case of $B = 0$. Expanding Eq. 51*a* leads to

$$1 - \frac{1}{2}\left(\frac{h\omega}{V}\right)^2 + \frac{1}{24}\left(\frac{h\omega}{V}\right)^4 + \ldots + \frac{(-1)^n}{(2n)!}\left(\frac{h\omega}{V}\right)^{2n} + \ldots ,$$

which is to be compared with Eq. 52*a*; that is,

$$1 - \frac{1}{2}\left(\frac{h\omega}{V}\right)^2 + \frac{1}{4}\left(\frac{h\omega}{V}\right)^4 + \ldots + \frac{2(-1)^n}{(4)^{2n}}\left(\frac{h\omega}{V}\right)^{2n} + \ldots .$$

The expansion of Eq. 51*b* with $B = 0$ leads to

$$\left(\frac{h\omega}{V}\right) - \frac{1}{6}\left(\frac{h\omega}{V}\right)^3 + \frac{1}{120}\left(\frac{h\omega}{V}\right)^5 + \ldots + \frac{(-1)^{2n+1}}{(2n+1)!}\left(\frac{h\omega}{V}\right)^{2n+1} + \ldots ;$$

and Eq. 52*b* yields

$$\left(\frac{h\omega}{V}\right) - \frac{1}{4}\left(\frac{h\omega}{V}\right)^3 + \frac{1}{16}\left(\frac{h\omega}{V}\right)^5 + \ldots + \frac{(-1)^{2n+1}}{(4)^n}\left(\frac{h\omega}{V}\right)^{2n+1} + \ldots .$$

From the expansions for the case of $B = 0$, it is obvious for a given h and V that the difference between the lumped- and distributed-parameter models increases as ω increases. Furthermore, the difference is greater in the imaginary term than in the real term; thus, by examining the magnitude and phase of $T_c(h, j\omega)$ relative to $T_c(0, j\omega)$ by the two methods, errors in the phase would occur at lower frequencies more often than errors in the magnitude. An approximation for the maximum value of the parameter $(h\omega/v)$ that one can use in the distributed-parameter model was obtained by displaying graphically the quantities $E[(h\omega/V), (hB/V)]$ and $\angle E[(h\omega/V), (hB/V)]$, which are defined by

$$E\left(\frac{h\omega}{V}, \frac{hB}{V}\right) \equiv \left\{\left|\frac{T_c(h, j\omega)}{T_c(0, j\omega)}\right|_{\text{approximate}} - \left|\frac{T_c(h, j\omega)}{T_c(0, j\omega)}\right|_{\text{exact}}\right\} \Bigg/ \left|\frac{T_c(h, j\omega)}{T_c(0, j\omega)}\right|_{\text{exact}} , \quad (53)$$

$$\angle E\left(\frac{h\omega}{V}, \frac{hB}{V}\right) \equiv \angle\left[\frac{T_c(h, j\omega)}{T_c(0, j\omega)}\right]_{\text{exact}} - \angle\left[\frac{T_c(h, j\omega)}{T_c(0, j\omega)}\right]_{\text{approximate}} , \quad (54)$$

where the subscript "exact" refers to the distributed model and "approximate" refers to the lumped model.

Figures 19 through 22 are the presentation of Eqs. 53 and 54 with B and ω as parameters and h/V as the independent variable. Postulating that it is desired to have an error in the angles of less than 0.1 radian, then it is observed that values of $h\omega/V \leqq 1$ always satisfy this requirement. Furthermore, the error in the magnitude remains less than 5% for $h\omega/V \leqq 1$.

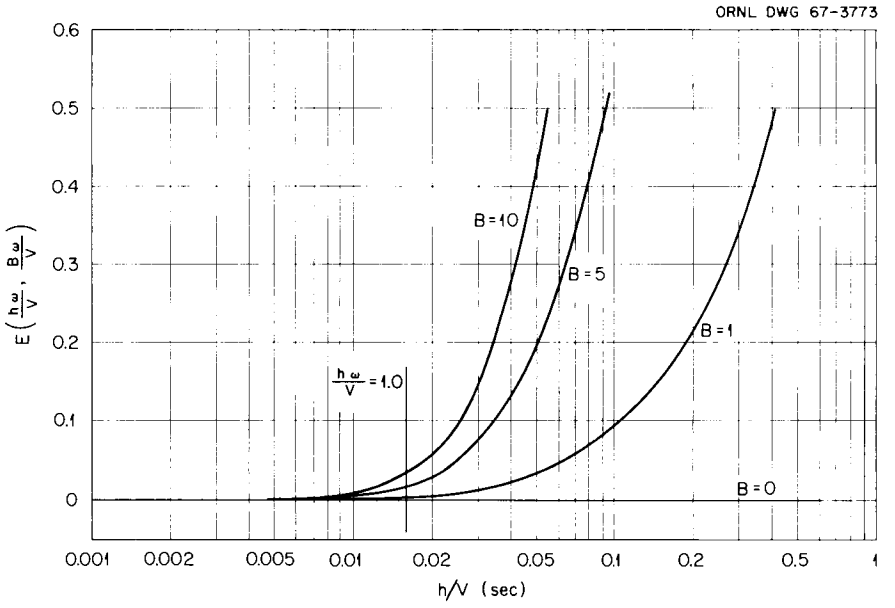

Fig. 19. Error in the Magnitude of the Outlet to the Inlet Coolont Temperature Transfer Function at a Frequency of 10 cps.

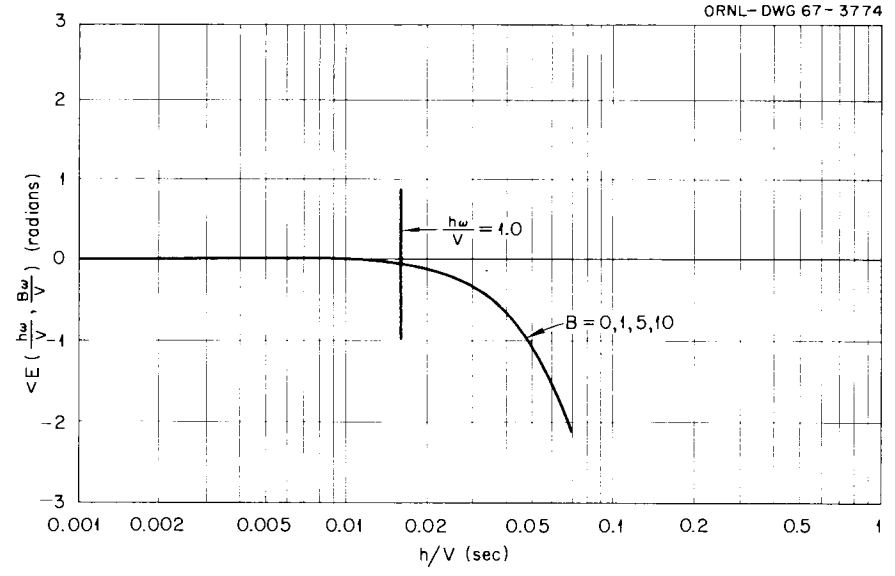

Fig. 20. Error in the Phase of the Outlet to the Inlet Coolant Temperature Transfer Function at a Frequency of 10 cps.

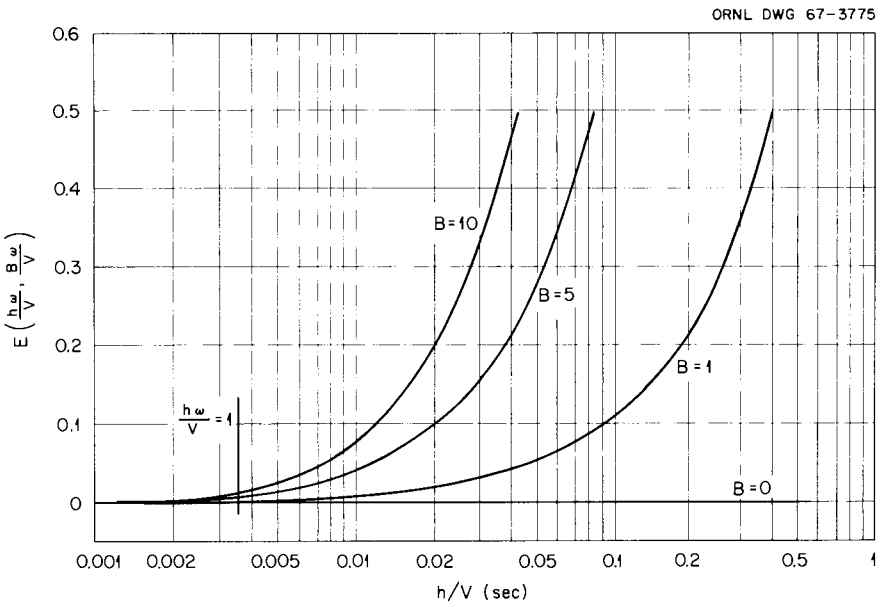

Fig. 21. Error in the Magnitude of the Outlet to the Inlet Coolant Temperature Transfer Function at a Frequency of 50 cps.

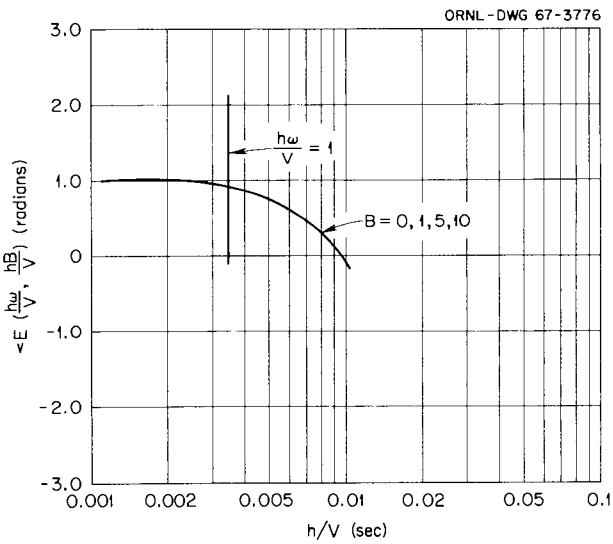

Fig. 22. Error in the Phase of the Outlet to the Inlet Coolant Temperature Transfer Function at a Frequency of 50 cps.

5.2 Model Equations

5.2.1 Neutronic Model

The basic model assumed to be valid for this study is the one-velocity diffusion model; that is,

$$\nabla \cdot D\nabla\phi + [\nu(1-\beta)\Sigma_f - \Sigma_a]\phi + \sum_{i=1}^{6} \lambda_i C_i - V^{-1}\frac{\partial\phi}{\partial t} = 0 , \tag{55a}$$

$$\beta_i \nu\Sigma_f\phi - \lambda_i C_i - \frac{\partial C_i}{\partial t} = 0 , \tag{55b}$$

for $i = 1, 2, \ldots, 6$. An approximate solution for ϕ and C_i is assumed to be of the form

$$\phi(\mathbf{r}, t) \approx N(t)\, H(\mathbf{r}) , \tag{56a}$$

$$C_i(\mathbf{r}, t) \approx T^i(t)\, Z^i(\mathbf{r}) , \tag{56b}$$

for $i = 1, 2, \ldots, 6$. Then $H(\mathbf{r})$ and $Z^i(\mathbf{r})$ are specified, which reduces Eqs. 55*a* and 55*b* to time-dependent equations. When the approximate solutions (Eqs. 56*a* and 56*b*) are substituted into Eqs. 55*a* and 55*b*, a residue $R(\mathbf{r}, t)$ is obtained which will approach zero at each point in phase space as the approximate solution approaches the exact solution. Since the primary interest is in the total neutron balance (for an approximate solution), we choose the time-varying coefficients in Eq. 56 so that the total residue over phase space is zero. This is accomplished by using the method of weighted residuals:[14] multiply the residue by some weighting function, say $\psi(\mathbf{r}, t)$, and choose the parameters N and T^i of Eq. 56 so that the total weighted residual is zero; that is,

$$\int_{t_1}^{t_2} dt \int_{\mathbf{r}} d\mathbf{r}[\psi(\mathbf{r}, t)\, R(\mathbf{r}, t)] = 0 . \tag{57}$$

If ψ is chosen as the adjoint function, the weighted residual method becomes the variational method.[14] Since the requirement that the total weighted residual be zero may lead to unrealistic solutions, we require instead that the integral in Eq. 57 be an extremum, which is the variational principle.[15] Thus, define J to be

---

[14] M. Becker, *The Principles and Applications of Variational Methods*, Research Monograph No. 27, MIT Press, Cambridge, Mass., 1964.

[15] D. S. Selengut, "Variational Analysis of Multi-Dimensional Systems," *Nucl. Phys. Res. Quart. Rept. Oct., Nov., Dec., 1958*, HW-59126, pp. 89–124 (January 1959).

$$J(\psi, \phi) \equiv \int_{t_1}^{t_2} dt \int_r dr \; \psi \left\{ \nabla \cdot D \nabla \phi + [\nu(1 - \beta) \Sigma_f - \Sigma_a] \phi + \sum_{i=1}^{6} \lambda_i C_i - V^{-1} \frac{\partial \phi}{\partial t} \right\} , \tag{58}$$

and require J to be an extremum subject to the constraints[6]

$$\beta_i \nu \Sigma_f \phi - \lambda_i C_i - \frac{\partial C_i}{\partial t} = 0 \tag{59}$$

for $i = 1, 2, \ldots, 6$. The requirement that J be an extremum leads to an equation for ψ, with appropriate constraint equations, which is an adjoint equation.

The adjoint equations are equally as difficult as Eq. 55; hence, an approximate solution to ψ is assumed to be

$$\psi(\mathbf{r}, t) \approx N^*(t) H^*(\mathbf{r}) . \tag{60}$$

For small transients about some reference state (assumed steady), reasonable spatial functions (modes) for ϕ and ψ are the actual flux and adjoint (importance) flux existing in the steady state. Therefore, since the one-velocity steady-state model is self-adjoint, H and H^* are taken to be

$$H(\mathbf{r}) = H^*(\mathbf{r}) = K \phi_0(\mathbf{r}) ,$$

where the subscript 0 refers to the steady state and K is some arbitrary constant chosen to make H have the desired units (power density, for example).

Equations for the time-dependent coefficients of Eq. 56 were obtained as follows:

1. Multiply each term of Eq. 59 by a Lagrange multiplier, say $L_i(\mathbf{r}, t)$ for $i = 1, 2, \ldots, 6$, and add the resultant expressions to the integrand of Eq. 58.
2. Substitute the assumed approximate solutions into the modified Eq. 58 and carry out the spatial integrations.
3. Require the resultant expression for J to be an extremum, which is the restricted variational principle.[5,6]

This procedure leads to the following equations for $N(t)$ and $T^i(t)$:[6]

$$\left(\int_r H^* V^{-1} H \, dr \right) \frac{dN}{dt} = \left(\int_r \{ -\nabla H^* \cdot D \nabla H - H^* [\Sigma_a - (1 - \beta) \nu \Sigma_f] H \} \, dr \right) N + \sum_{i=1}^{6} \lambda_i \left(\int_r H^* Z^i \, dr \right) T^i , \tag{61a}$$

$$\left(\int_r Z^{*i} Z^i \, dr \right) \frac{dT^i}{dt} = \beta_i \left(\int_r Z^{*i} \nu \Sigma_f H \, dr \right) N - \lambda_i \left(\int_r Z^{*i} Z^i \, dr \right) T^i , \tag{61b}$$

for $i = 1, 2, \ldots, 6$, where Z^{*i} was introduced by assuming separability for the Lagrange multipliers.

Since $H(\mathbf{r})$ is $\phi_0(\mathbf{r})$, and H^* is the same as $H(\mathbf{r})$, it follows that

$$Z^i(\mathbf{r}) = Z^{*i}(\mathbf{r}) = \frac{\beta_i}{\lambda_i} \nu\Sigma_f H(\mathbf{r}) \,. \tag{62}$$

Define

$$\Lambda \equiv \frac{\int_{\mathbf{r}} H^* H \, d\mathbf{r}}{\int_{\mathbf{r}} H^* \nu\Sigma_f H \, d\mathbf{r}} = \frac{\int_{\mathbf{r}} (H^* H / \overline{\nu\Sigma_f} V) \, d\mathbf{r}}{\int_{\mathbf{r}} H^* H \, d\mathbf{r}} \,, \tag{63a}$$

where

$$\overline{\nu\Sigma_f} \equiv \frac{\int_{\mathbf{r}} H^* \nu\Sigma_f H \, d\mathbf{r}}{\int_{\mathbf{r}} H^* H \, d\mathbf{r}} \,; \tag{63b}$$

then, with the aid of Eq. 62, Eq. 61 can be written as

$$\Lambda \frac{dN}{dt} = \left\{ \frac{\int_{\mathbf{r}} [\,(- \nabla H^* \cdot D \nabla H - H^* \Sigma_a H + H^* \nu\Sigma_f H) / \overline{\nu\Sigma_f}]}{\int_{\mathbf{r}} H^* H \, d\mathbf{r}} \right\} N - \beta N + \sum_{i=1}^{6} \beta_i T^i \,, \tag{64a}$$

$$\frac{dT^i}{dt} = \beta_i N - \lambda_i T^i \,. \tag{64b}$$

Define

$$\overline{DB^2} \equiv \frac{\int_{\mathbf{r}} \nabla H^* \cdot D \nabla H \, d\mathbf{r}}{\int_{\mathbf{r}} H^* H \, d\mathbf{r}} \,,$$

$$\rho_L(\mathbf{r}, t) \equiv \frac{- \overline{DB^2} - \Sigma_a + \nu\Sigma_f}{\overline{\nu\Sigma_f}} \,;$$

then Eq. 64*a* becomes

$$\Lambda \frac{dN}{dt} = \frac{\int_{\mathbf{r}} H^* \rho_L H \, d\mathbf{r}}{\int_{\mathbf{r}} H^* H \, d\mathbf{r}} N - \beta N + \sum_{i=1}^{6} \beta_i T^i \,, \tag{65}$$

where ρ_L is to be interpreted as the local reactivity. If H is chosen to be the steady-state flux, it is obvious from Eq. 56 that

$$N(0) = T^1(0) = \ldots = T^6(0) = 1 ,$$

and, from Eq. 65,

$$\int_r H^* \rho_L(\mathbf{r}, t = 0) H \, d\mathbf{r} = 0 .$$

Assume small deviations about the steady state and write

$$\rho_L(\mathbf{r}, t) = \rho_L(\mathbf{r}, 0) + \rho_L'(\mathbf{r}, t) ,$$

$$N(t) = N(0) + N'(t) = 1 + N'(t) ,$$

$$T^i(t) = T^i(0) + T^{i\prime}(t) = 1 + T^{i\prime}(t) ;$$

then Eqs. 65 and 64*b* become (ignoring products of small terms)

$$\Lambda \frac{dN'}{dt} = \left(\frac{\int_r H^* \rho_L' H \, d\mathbf{r}}{\int_r H^* H \, d\mathbf{r}} \right) - \beta N' + \sum_{i=1}^{6} \beta_i T^{i\prime} , \tag{66a}$$

$$\frac{dT^{i\prime}}{dt} = \beta_i N' - \lambda_i T^{i\prime} . \tag{66b}$$

Laplace transform Eq. 66 to obtain (dropping primes)

$$\left[\Lambda s + \beta - \sum_{i=1}^{6} \frac{\lambda_i \beta_i}{s + \lambda_i} \right] N(s) = \left[\frac{\int_r H^* \rho_L(\mathbf{r}, s) H \, d\mathbf{r}}{\int_r H^* H \, d\mathbf{r}} \right] . \tag{67}$$

An alternate useful form of Eq. 67 is

$$\left[\Lambda s + \beta - \sum_{i=1}^{6} \frac{\lambda_i \beta_i}{s + \lambda_i} \right] P(s) = \left[\frac{\int_r H^* \rho_L(\mathbf{r}, s) H \, d\mathbf{r}}{\int_r H^* H \, d\mathbf{r}} \right] P_0 , \tag{68}$$

where $P(s)$, given by

$$P(s) = P_0 N(s) ,$$

represents the variation in the power level.

In the application of Eq. 66 or 68, the local reactivity will be taken as the sum of reactivities due to changes in local temperature, voids, etc. As an example, consider a light-water-reflected-moderated-cooled stationary fueled reactor. Suppose that changes in the temperature of the fuel and water in the fueled region as well as changes in the temperature of the water in the nonfueled region affect the total reactivity of the system. Then the local reactivity ρ_L will be taken (in part) as

$$\rho_L(\mathbf{r}, s) = \alpha_{W,M}(\mathbf{r}) \delta T_{W,M}(\mathbf{r}, s) + \alpha_{W,F}(\mathbf{r}) \delta T_{W,F}(\mathbf{r}, s) + \alpha_F(\mathbf{r}) \delta T_F(\mathbf{r}, s) , \tag{69}$$

where the subscript (W,M) is for the water in the nonfueled region, (W,F) is for the water in the fueled region, (F) is for the fuel, and α, the temperature reactivity coefficient, is zero outside the indicated regions.

The temperature coefficients in Eq. 69 are not necessarily those that would be calculated or measured. For example, the temperature coefficient is generally obtained by making a step change in temperature δT (independent of position) and noting the total change in reactivity ρ; then the temperature coefficient α is obtained from

$$\alpha = \rho/\delta T \ .$$

For this example, suppose that the coefficient of interest is $\alpha_{W,M}$. Then the total reactivity is given by

$$\rho = \frac{\int_M H^* \alpha_{W,M} \delta T H \, d\mathbf{r}}{\int_{M+F} H^* H \, d\mathbf{r}} = \alpha \delta T \ ,$$

where α is the observed coefficient. For a constant $\alpha_{W,M}$ and δT in the nonfueled region,

$$\alpha_{W,M} = \alpha \frac{\int_M H^* H \, d\mathbf{r} + \int_F H^* H \, d\mathbf{r}}{\int_M H^* H \, d\mathbf{r}} \ ,$$

where M and F represent the nonfueled and fueled regions respectively.

Writing the local reactivity as

$$\rho_L = \sum_j \alpha_j \delta T_j + \rho_{\text{ext}} \ ,$$

where ρ_{ext} takes into account all quantities other than temperature which affect reactivity, Eq. 67 can be written as

$$\left(\Lambda s + \beta - \sum_{i=1}^{6} \frac{\lambda_i \beta_i}{s + \lambda_i} \right) N(s) = \sum_j \alpha_j \, \delta T_{j,\text{eff}} + \rho_{\text{ext}} \ , \tag{70}$$

where

$$\delta T_{j,\text{eff}} \equiv \frac{\int_{\mathbf{r}} H^* \delta T_j(\mathbf{r}, s) H \, d\mathbf{r}}{\int_{\mathbf{r}} H^* H \, d\mathbf{r}} \ . \tag{71}$$

Equations 70 and 71 are used for the neutronic model.

5.2.2 Thermodynamic Model

The model will become complete when an expression for $\delta T_j(\mathbf{r}, s)$ of Eq. 71 is specified. Thus, considering the system shown in Fig. 18, the temperature equations are

$$M_c \frac{\partial T_c}{\partial t} + d_c V_c \frac{\partial T_c}{\partial z} = a \dddot{P} + u V_c^{0.8} (T_s - T_c) , \tag{72}$$

$$M_s \frac{\partial T_s}{\partial t} = b \dddot{P} - u V_c^{0.8} (T_s - T_c) , \tag{73}$$

where one-dimensional flow has been assumed, and the subscripts c and s refer to the coolant and solid respectively. In the following equations,

$$\begin{aligned} V_c^{0.8}(t) &\approx V_{c0}^{0.8} \left(1 + \frac{\delta V_c}{V_{c0}}\right), \\ T_c(z, t) &= T_{c0}(z) + \delta T_c(z, t) , \\ T_s(z, t) &= T_{s0}(z) + \delta T_s(z, t) , \\ \dddot{P}(z, t) &= \dddot{P}_0(z) + \delta P(z, t) + S(t) , \end{aligned} \tag{74}$$

the subscript 0 refers to the steady state, and S is a noise-equivalent source which accounts for random fluctuations in the power. At steady state, Eqs. 72 and 73 reduce to

$$d_c V_{c0} \frac{\partial T_{c0}}{\partial z} = a \dddot{P}_0 + u V_{c0}^{0.8} (T_{s0} - T_{c0}) , \tag{75}$$

$$0 = b \dddot{P}_0 - u V_{c0}^{0.8} (T_{s0} - T_{c0}) . \tag{76}$$

Substitute Eq. 74 into Eqs. 72 and 73 and neglect products of the delta terms (assume small deviations about the mean) which, with the aid of Eqs. 75 and 76, yield

$$M_c \frac{\partial \delta T_c}{\partial t} + d_c V_{c0} \frac{\partial \delta T_c}{\partial z} + \frac{\dddot{P}_0}{V_{c0}} a \delta V_c = a(\delta \dddot{P} + S) + u V_{c0}^{0.8} (\delta T_s - \delta T_c) , \tag{77}$$

$$M_s \frac{\partial \delta T_s}{\partial t} = b(\delta \dddot{P} + S) - u V_{c0}^{0.8} (\delta T_s - \delta T_c) - b \dddot{P}_0 \frac{\delta V_c}{V_{c0}} . \tag{78}$$

Laplace transform Eqs. 77 and 78 and eliminate δT_s in Eq. 77, which leads to

$$d_c V_{c0} \frac{d\delta T_c}{dz} + \left[M_c s + u V_{c0}^{0.8} - \frac{(u V_{c0}^{0.8})^2}{M_s s + u V_{c0}^{0.8}} \right] \delta T_c + \dddot{P}_0 \left(a + \frac{b u V_{c0}^{0.8} \dddot{P}_0}{M_s s + u V_{c0}^{0.8}} \right) \frac{\delta V_c}{V_{c0}} = \left(a + \frac{b u V_{c0}^{0.8}}{M_s s + u V_{c0}^{0.8}} \right) (\delta \dddot{P} + S) . \quad (79)$$

From Eq. 79 it is evident that if a fluctuation in the coolant velocity is significant as a driving function for the power spectral density, then the magnitude of the driving function will be proportional to the square of the power. Examination of the experimental power spectral densities for the ORR and the HFIR, Figs. 5 and 16, clearly shows that this is not the case; therefore, the fluctuation in the coolant velocity is insignificant and hence will be ignored in this analysis. Then the equations which are used become

$$d_c V_{c0} \frac{d\delta T}{dz} + \left[M_c s + u V_{c0}^{0.8} - \frac{(u V_{c0}^{0.8})^2}{M_c s + u V_{c0}^{0.8}} \right] \delta T_c = \left[a + \frac{b u V_{c0}^{0.8}}{M_s s + u V_{c0}^{0.8}} \right] (\delta \dddot{P} + S) , \quad (80)$$

$$\delta T_s = \frac{b}{M_s s + u V_{c0}^{0.8}} (\delta \dddot{P} + S) + \frac{u V_{c0}^{0.8}}{M_s s + u V_{c0}^{0.8}} \delta T_c . \quad (81)$$

Let

$$a_1(s) \equiv \frac{1}{d_c V_{c0}} \left[M_c s + u V_{c0}^{0.8} - \frac{(u V_{c0}^{0.8})^2}{M_s s + u V_{c0}^{0.8}} \right] ,$$

$$a_2(s) \equiv \frac{1}{d_c V_{c0}} \left(a + \frac{b u V_{c0}^{0.8}}{M_s s + u V_{c0}^{0.8}} \right) ,$$

$$a_3(s) \equiv \frac{b}{M_s s + u V_{c0}^{0.8}} ,$$

$$a_4(s) \equiv \frac{u V_{c0}^{0.8}}{M_s s + u V_{c0}^{0.8}} ;$$

then Eqs. 80 and 81 can be written as

$$\delta T_c(z, s) = e^{-a_1(z-z_0)}\delta T_c(z_0, s) + a_2 e^{-a_1(z-z_0)} \int_{z_0}^{z_1} \{e^{a_1(z'-z_0)} \times [\delta \dddot{P}(z', s) + S(z', s)]\}\, dz' , \quad (82)$$

$$\delta T_s(z, s) = a_3[\delta \dddot{P}(z, s) + S(z, s)] + a_4 \delta T_c(z, s) , \quad (83)$$

where $\delta \dddot{P}$ and S have the same spatial dependence as the spatial weighting function H used in the neutronic model, and $\delta T_c(z_0, s)$ is the fluctuation in temperature of the coolant at the inlet of the reactor. Equations 82 and 83 are sufficient for the expansion of Eq. 71, and thus they complete the thermodynamic model.

5.2.3 Solution to the Thermodynamic and Neutronic Equations

From Eq. 14 it is evident that the power spectral density is proportional to the square of the mean power if the noise-equivalent source is negligible relative to the external reactivities; therefore, the noise-equivalent source S in Eqs. 82 and 83 will be neglected, since the experimental power spectral densities in the ORR and the HFIR are proportional to the square of the power. In accordance with Eq. 71, $\delta T_{c,\mathrm{eff}}$ and $\delta T_{s,\mathrm{eff}}$ are given by (assuming a flat power distribution in the radial direction)

$$\delta T_{c,\mathrm{eff}} = \frac{\int_{z_0}^{z_u} H^* \delta T_c(z, s) H\, dz}{\int_{z_0}^{z_u} H^* H\, dz} , \quad (84)$$

$$\delta T_{s,\mathrm{eff}} = \frac{\int_{z_0}^{z_u} H^* \delta T_s(z, s) H\, dz}{\int_{z_0}^{z_u} H^* H\, dz} , \quad (85)$$

where $(z_u - z_0)$ is the height of the core in the direction of flow, and H and H^* are the weighting functions previously defined. Let

$$\delta \dddot{P}(z, s) = KH(z)\, N(s) , \quad (86)$$

where K is a constant which converts $H(z)$ to the steady-state power density, and $N(s)$ is the fluctuating component of the flux. Define

$$T_{j,\mathrm{eff}}(s) \equiv \delta T_{j,\mathrm{eff}}(s) \ ;$$

then Eqs. 84 and 85 (with the aid of Eqs. 82, 83, and 86) can be written as

$$DT_{c,\mathrm{eff}}(s) = A\delta T_c(z_0, s) + BN(s) \ , \tag{87}$$

$$DT_{s,\mathrm{eff}}(s) = EN(s) + F\delta T_c(z_0, s) \ , \tag{88}$$

where

$$D = \int_{z_0}^{z_u} H^* H \, dz \ ,$$

$$A = \int_{z_0}^{z_u} H^* e^{-a_1(z-z_0)} H \, dz \ ,$$

$$B = \int_{z_0}^{z_u} H^* \{a_2 e^{-a_1(z-z_0)} \int_{z_0}^{z} [e^{a_1(z'-z_0)} KH] \, dz' \} H \, dz \ ,$$

$$E = \int_{z_0}^{z_u} H^* \{a_3 KH + a_4 a_2 e^{-a_1(z-z_0)} \int_{z_0}^{z} [e^{a_1(z'-z_0)} KH] \, dz' \} H \, dz \ ,$$

$$F = \int_{z_0}^{z_u} H^* a_4 e^{-a_1(z-z_0)} H \, dz \ ,$$

and all other terms have been defined previously. Equations 70, 87, and 88 are then put in matrix form; that is,

$$AX = Y \ , \tag{89}$$

where A is the square matrix

$$A = \begin{bmatrix} \left(\Lambda s + \beta - \sum_{i=1}^{6} \frac{\lambda_i \beta_i}{s + \lambda_i}\right) & -\alpha_c & -\alpha_s \\ -B & D & 0 \\ -E & 0 & D \end{bmatrix} ,$$

X is the column matrix

$$X = \begin{bmatrix} N(s) \\ T_{c,\mathrm{eff}}(s) \\ T_{s,\mathrm{eff}}(s) \end{bmatrix},$$

and Y is the column matrix

$$Y = \begin{bmatrix} \rho_{\mathrm{ext}} \\ A\delta T_c(z_0, s) \\ F\delta T_c(z_0, s) \end{bmatrix},$$

which is the driving "function" matrix.

The elements in A and Y were calculated (or specified) using a CDC 1604 computer. Then Eq. 89 was solved for the elements of X using matrix techniques.

ORNL-4149
UC-80 – Reactor Technology

INTERNAL DISTRIBUTION

1. Biology Library
2–4. Central Research Library
5–6. ORNL – Y-12 Technical Library Document Reference Section
7–41. Laboratory Records Department
42. Laboratory Records, ORNL R.C.
43. S. J. Ball
44. D. S. Billington
45. F. T. Binford
46. A. L. Boch
47. C. J. Borkowski
48. J. B. Bullock
49. C. D. Cagle
50. T. E. Cole
51. B. L. Corbett
52. J. A. Cox
53. S. J. Cromer
54. F. L. Culler
55. H. P. Danforth
56. J. R. Engel
57. E. P. Epler
58. D. N. Fry
59. C. S. Harrill
60. P. N. Haubenreich
61. W. H. Jordan
62. R. T. King
63. R. C. Kryter
64. C. E. Larson
65. H. G. MacPherson
66. R. V. McCord
67. F. R. McQuilkin
68. S. E. Moore
69. L. C. Oakes
70. R. B. Parker
71. A. M. Perry
72–81. J. C. Robinson
82–91. D. P. Roux
92. G. S. Sadowski
93. M. J. Skinner
94. L. E. Stanford
95. R. S. Stone
96. E. Straker
97. W. H. Tabor
98. J. R. Tallackson
99. S. C. Weaver
100. A. M. Weinberg
101. R. C. Weir
102. M. L. Winton

EXTERNAL DISTRIBUTION

103. S. H. Hanauer, Dept. of Nuclear Engineering, University of Tennessee, Knoxville
104. T. W. Kerlin, Dept. of Nuclear Engineering, University of Tennessee, Knoxville
105. B. R. Lawrence, AAEC, Private Mailbag, Sutherland, NSW, Australia
106–110. F. C. Legler, Reactor Development Division, AEC, Washington
111. S. E. Stephenson, Dept. of Electrical Engineering, University of Arkansas
112. Dieter Stegemann, Institut fur Neutronenphysik und Reaktortechnik, Kernforschungszentrum, Karlsruhe, Germany
113. A. Z. Akcasu, University of Michigan
114. J. A. Swartout, Union Carbide Corporation, New York, N.Y.
115. Laboratory and University Division, AEC, ORO
116–375. Given distribution as shown in TID-4500 under Reactor Technology category (25 copies – CFSTI)